

# SIMULATION OF ROTARY REACTOR

## A DISSERTATION

*Submitted in partial fulfillment of the  
requirements for the award of the degree  
of*

**MASTER OF TECHNOLOGY**

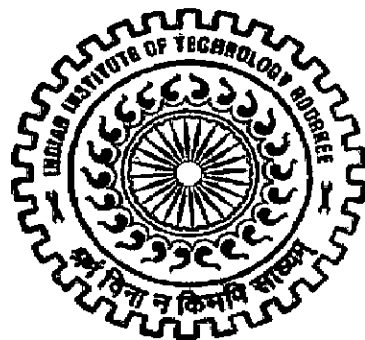
*in*

**CHEMICAL ENGINEERING**

**(With Specialization in Computer Aided Process Plant Design)**

By

**SHOEB AHMAD**



**DEPARTMENT OF CHEMICAL ENGINEERING  
INDIAN INSTITUTE OF TECHNOLOGY ROORKEE  
ROORKEE-247 667 (INDIA)**

**JUNE, 2006**

## **CANDIDATE'S DECLARATION**

---

---

I, hereby, certify that the work which is being presented in the thesis entitled "**SIMULATION OF ROTARY REACTOR**" in partial fulfillment of the requirement for the award of the degree of **Master of Technology** in **Chemical Engineering** with specialization in **Computer Aided Process Plant Design (CAPPD)**, and submitted in the **Department of Chemical Engineering** of **Indian Institute of Technology Roorkee**, Roorkee. This is an authentic record of my own work carried out during the period from July 2005 to June 2006 under the supervision of **Dr. Surendra Kumar**, Professor, Department of Chemical Engineering, Indian Institute of Technology Roorkee, Roorkee.

The matter presented in this thesis has not been submitted for the award of any other degree/diploma of this or any other Institute/University.

Date : June 29, 2006

Place : Roorkee

  
(Shoeb Ahmad)

---

---

## **CERTIFICATE**

This is to certify that the above statement made by the candidate is correct to the best of my knowledge.



(Dr. Surendra Kumar)

Professor

Chemical Engineering Department

Indian Institute of Technology, Roorkee

Roorkee, 247667

## **ABSTRACT**

Rotary reactor is employed by industries to carry out a wide variety of material processing. A steady state one dimensional mathematical model was developed to predict mass transfer and heat transfer from freeboard gas to the bed or wall of the rotary reactor. The purpose of the model is a better understanding of calcination of limestone and activation of charcoal.

The heat transfer equations incorporated direct gas to surface exchange, reflection of the gas radiation by the wall and reactor wall to solid exchange. A simplified mathematical model consisting of five ODEs, algebraic equations and set of boundary conditions has been proposed. The model was simulated by RKF method using MATLAB (Version 7.01).

The solution predicts solid, freeboard gas and wall axial temperature profile as well as mass variations in the solid and freeboard gas due to reaction and solid drying. The resulting profile is then compared with the experimental data available in the literature. Burn off and production has been defined to measure the performance of the reactor. Sensitivity analysis results permits us to identify the operating variables that can be optimized.

## **ACKNOWLEDGEMENT**

I wish to express my sincere thanks and sense of gratitude to my project guide, Dr. Surendra Kumar, for his scholarly guidance, encouragement and discussion for this report. I am thankful to Dr. (Mrs.) Shashi for her invaluable help during the course of this dissertation.

I would like to thank Dr. Sri Chand, Chairman DRC and Head, Department of Chemical Engineering, IIT Roorkee, for providing me the necessary facilities for the compilation of this report.

Many thanks are due to my friends Fahad, Bansal, Gaurav, Anees, Atif, Qazi, Sachin and Asad for their indispensable help in the completion of this work. My special thanks are due to Sheeba Madam for her immense help and motivation during my days in RER Lab.

The Library In-charge, Mrs Verma, also deserve special thanks for placing the library at my disposal whenever required. I am grateful to all the members of RER Lab, especially Rahman Sb, Tripta Didi, Mange Ram Ji and Salman Zafar for their cooperation and support during the M.Tech program.

This report saw the light of the day only due to the encouragement and unflinching support and love of my parents, sisters and brothers.

Utmost thanks are due to the Almighty, for providing me the knowledge and wisdom for the successful completion of this dissertation.

**(Shoeb Ahmad)**

# CONTENTS

<b>ABSTRACT</b>	i
<b>ACKNOWLEDGEMENT</b>	ii
<b>CONTENTS</b>	iii
<b>LIST OF FIGURES</b>	vi
<b>NOMENCLATURE</b>	viii
<b>CHAPTER I. INTRODUCTION</b>	<b>1</b>
1.1 BED BEHAVIOUR IN ROTARY REACTOR	7
1.1.1 Slipping Motion	8
1.1.2 Cascading (Tumbling) Motion	9
1.1.3 Cataracting Motion	10
1.2 DESIGN OF ROTARY REACTOR	10
1.2.1 Thermal decomposition example	11
1.2.2 Reactor example	11
1.2.3 Horizontal rotating cylinder with a partition plate and guide plates	12
1.2.4 Equation to estimate rate of solids movement	12
1.3 MODELLING OF ROTARY REACTOR (PREVIOUS WORK)	19
1.3.1 The two dimensional thermal model applied to the bed	22
<b>CHAPTER II. LITERATURE REVIEW</b>	<b>25</b>
<b>CHAPTER III. MODELLING OF ROTARY REACTOR</b>	<b>43</b>
3.1 CHEMICAL REACTION KINETICS	44
3.2 MODEL DEVELOPMENT	46
3.2.1 Mass balance of moisture into the control volume	46
3.2.2 Mass balance for the solid	50

3.2.3	Mass balance for the gas	51
3.3	ENERGY BALANCES	53
3.3.1	Energy exchange between gas and solid	53
3.3.2	Energy exchange between wall and gas	54
3.3.3	Energy exchange between wall and solid due to wall radiation	55
3.3.4	Energy exchange between wall and wall due to wall radiation	56
3.3.5	Energy exchange between wall and solid due to solid radiation	56
3.3.6	Energy balance for the gas	57
3.3.7	Energy balance for the solid	59
3.3.8	Energy balance for the wall	61
3.3.9	Boundary conditions and Initial conditions	62
3.4	STEADY STATE MODELS FOR ROTARY REACTOR	63
3.5	Estimation of Reactor Geometric Parameter	64
<b>CHAPTER</b>	<b>IV. RESULTS AND DISCUSSIONS</b>	<b>69</b>
4.1	INTRODUCTION	69
4.2	ALGORITHM	69
4.3	CHARCOAL ACTIVATION	70
4.3.1	Data and correlations	70
4.3.2	Flow profile along the length of reactor	71
4.3.3	Temperature Profile along the length of reactor	78
4.4	CALCINATION OF LIMESTONE	83
4.4.1	Data and correlations	83
4.4.2	Flow profile along the length of reactor	85
4.4.3	Temperature profile along the length of reactor	91
4.5	SENSITIVITY ANALYSIS	97

<b>CHAPTER V.</b>	<b>CONCLUSIONS AND RECOMMENDATIONS</b>	105
5.1	CONCLUSIONS	105
5.2	RECOMMENDATIONS OF FUTURE WORK	106
<b>REFERENCES</b>		107

## LIST OF FIGURES

<b>Figure 1.1</b>	Schematic of Rotary Kiln	5
<b>Figure 1.2</b>	Granular flow in the transverse plane	5
<b>Figure 1.3</b>	Horizontal rotary gas/solid contactor for single movement	13
<b>Figure 1.4</b>	Cross section of one side of the partition plate	13
<b>Figure 1.5</b>	Movement of solid during one revolution of the cylinder	17
<b>Figure 1.6</b>	Sketch showing how to achieve (a) longer plug flow reactor and (b) an approach to mixed flow of solids	17
<b>Figure 2.1</b>	Thermal resistance model	33
<b>Figure 3.1</b>	Reactor scheme	47
<b>Figure 3.2</b>	Cross-sectional area of the control volume of the reactor	65
<b>Figure 4.1</b>	Moisture profile along the length	73
<b>Figure 4.2</b>	Gas flow profile along the length	73
<b>Figure 4.3</b>	Solid flow profile along the length	75
<b>Figure 4.4</b>	Gas temperature profile along the length of reactor	79
<b>Figure 4.5</b>	Solid temperature profile along the length of reactor	79
<b>Figure 4.6</b>	Wall temperature profile along the length of reactor	81
<b>Figure 4.7</b>	Temperature profile of solid wall and gas in the reactor	81
<b>Figure 4.8</b>	Gas flow profile along the length of Reactor	87



<b>Figure 4.9</b>	Moisture flow profile along the length of Reactor	87
<b>Figure 4.10</b>	Solid flow profile along the length of Reactor	89
<b>Figure 4.11</b>	Gas temperature profile	93
<b>Figure 4.12</b>	Solid temperature profile	93
<b>Figure 4.13</b>	Wall temperature profile	95
<b>Figure 5.1</b>	Burn off and production vs. residence time	99
<b>Figure 5.2</b>	Burn off and production vs. gas flow rate	99
<b>Figure 5.3</b>	Burn off and production vs. solid input temperature	101
<b>Figure 5.4</b>	Burn off and production vs. water vapor flow rate	101
<b>Figure 5.5</b>	Burn off and Production vs. solid flow rate	103

# NOMENCLATURE

$x_{CaCO_3}$	conversion of $CaCO_3$ [-]
$A$	Gas-solid surface per unit length [ $m^2/m$ ]
$C_g$	heat capacity of gas [J/kg.K]
$C_s$	heat capacity of solid [J/kg.K]
$C_v$	heat capacity of water vapor [J/kg.K]
$D$	internal diameter of the reactor [m]
$F_{ws}$	wall to solid view factor [-]
$F_{ww}$	wall to wall view factor [-]
$h_{gs}$	gas to solid heat transfer coefficient [ $W/m^2K$ ]
$h_{gw}$	gas to wall heat transfer coefficient [ $W/m^2K$ ]
$h_t$	heat transfer coefficient for drying process [ $W/m^2K$ ]
$H_v$	heat of vaporization of water [J/kg]
$h_{ws}$	wall to solid heat transfer coefficient [ $W/m^2K$ ]
$k_c$	first order reaction rate constant [ $s^{-1}$ ]
$L$	length of reactor [m]
$L_{fi}$	free wall surface [ $m^2/m$ ]
$L_{cu}$	cord length [ $m^2/m$ ]
$L_{es}$	covered wall surface [ $m^2/m$ ]
$N$	rotational speed [rpm]
$Q_a$	steam flow rate [kg/s]
$Q_g$	gas flow rate [kg/s]
$Q_h$	moisture flow rate [kg/s]
$Q_s$	Solid flow rate [kg/s]
$R$	Universal gas constant 8.314 [J/mol- $^{\circ}C$ ]
$S$	rotary reactor inclination slope [-]
$t$	residence time [sec]
$T_a$	temperature of surrounding [K]

$T_g$	temperature of gas [K]
$T_s$	temperature of solid [K]
$T_w$	temperature of wall [K]
$V_g$	velocity of gas [m/s]
$V_s$	velocity of solid [m/s]
$\Delta H$	heat of reaction [J/kg]

Greek symbols:

$\gamma_s$	activation reaction rate [ kg/s-m]
$\sigma$	Boltzman constant $5.57E-8$ [W/m <sup>2</sup> .K <sup>4</sup> ]
$\rho$	density of solid [kg/m <sup>3</sup> ]
$v_s$	velocity of solid [m/s]
$v_g$	velocity of gas [m/s]
$\epsilon_g$	emissivity of gas [-]
$\epsilon_s$	emissivity of solid [-]
$\epsilon_w$	emissivity of wall [-]

Subscripts

a	water
co	carbon monoxide
g	gas
h	moisture
i	component
s	solid
t	time
w	wall
z	axial length
v	vaporization

**INTRODUCTION**

---

---

Rotary reactor is simply a rotating drum which varies greatly in size, types of internals, rotating speed and fill level. Some rotary reactors are inclined slightly, with the granular material entering at the upper end and flowing by gravity to the lower end. Some rotary reactor are cylinder without any internals, while others may contain flight on the inside surface of the wall, the flight lift and drop the particles into the gas stream. Lifters are common in rotary dryers where increasing the contact between the particles and the gas stream is beneficial. Rotary reactor are employed by industry to carry out a wide variety of material processing, for example, calcining of lime stone, reduction of ore, clinkering of cementitious material, reclamation of hydrated lime, calcining of petroleum coke, etc . This widespread usage can be attributed to factors such as the ability to handle varied feed stock, e.g., slurries of granular material having large variation in particle size, or the ability to maintain distinct environment, e.g. reduction condition within the bed coexisting in the oxidizing freeboard. The general long residence time of the material within the reactor, typically one hour or greater, aids in achieving an acceptably uniform product, there is considerable scope for improving this aspect of reactor performance. An initial step toward doing so is to achieve a more quantitative understanding of transport phenomena within the bed material as it passes along the reactor.

Rotary reactors are ubiquitous fixtures of the chemical process industries. Despite challenges from newer and more specialized gas-solids reactor, they continue to find application in drying, sintering, heating, calcining reducing, and roasting. Rotary reactor can handle feed stocks with broad particle size distributions or whose physical properties change significantly during processing, while the long residence time of the material within the reactor promote uniform product quality. In addition, dirt fuels often are utilized without serious product contamination, and multiple fuel capability is possible. Because a thorough understanding of the processes occurring within the rotary reactor has not been a prerequisite for their apparently satisfactory operation, research has not

progressed apace with competing, less tolerant, reactor. Until all the internal processes are understood and become predictable, rotary reactor will remain in the position of operating below their optimal performance in an increasingly sophisticated marketplace. Typically, in moving through the reactor, the bed material passes through a low temperature drying zone, a heating zone to bring it up to reaction temperature and a reactor zone. Thus, individual bed particles undergo heat and mass transfer (drying), heating only (heating zone), and heat and mass transfer with reaction (reaction zone). The heating zone may occupy a significant portion of the reactor length, while in the other two zones; heat transfer may be the rate controlling process.

In most rotary reactor operation, the objective is to drive specific bed reaction which, for either kinetics or thermodynamic reasons, often requires high bed temperature as high as 1200°C. The energy to raise the bed temperature to require level for reaction and in some instances, for example the endothermic calcinations of lime stone, to drive the reactions themselves, is extracted from combustion of hydrocarbon fuel in the freeboard. Heat transfer from the freeboard to the bed is rather complex and occur by all the path and processes shown in Figure 1.1.

The analytical tools for handling the phenomena occurring within the freeboard space have been readily available, for example the zone method for determining radiative heat transfer or commercial software for calculating fluid flow (and occasionally combustion processes as well. Although numerous rotary reactor models have been proposed, virtually all of these assume that, at each axial position along the reactor, the bed is well mixed in transverse plane; i.e. material is isothermal over any transverse section of the reactor. However many reactor operations experience considerable difficulty in achieving a uniform product, one example being lime kilns which experience chronic problems in preventing dead-burning of large particles while fully calcining the finer particles. Evidence such as this, as well as operator experience, suggests that a substantial transverse temperature non uniformity is generated within the bed. Thus the well-mixed assumption, although expedient, to the modeling of the rotary reactor, is

clearly deficient because it ignores the motion of the bed in the transverse plane or, more precisely, because it ignores the effect of the motion on the redistribution within the bed material of energy absorbed at the bed-freeboard interfacial surfaces.

Heat transfer within the bed material occurs by the same mechanisms as in any packed bed; i.e. particle-to-particle conduction and radiation, as well as interstitial gas to particle convection. However, the movement of the granular material superimposes an advective component for energy transport which has the potential to dominate overall heat transfer. The transverse bed motion in rotary reactor, e.g. cataracting, cascading, rolling, slumping etc depend on the rotation rate, degree of fill and rheology of the particles. Although industrial reactor may be operated in the slumping mode, it is usually more desirable to achieve the rolling mode in order to take advantage of improved mixing of particle along with faster surface renewal at exposed bed surface. For the rolling mode of bed material is characterized by the two distinct region shown Figure 1.2., the thinner active layer which is formed as the granular material flows down the sloping upper bed surface and the much thicker 'plug flow' region where the material is carried upward by the rotating wall of the reactor.

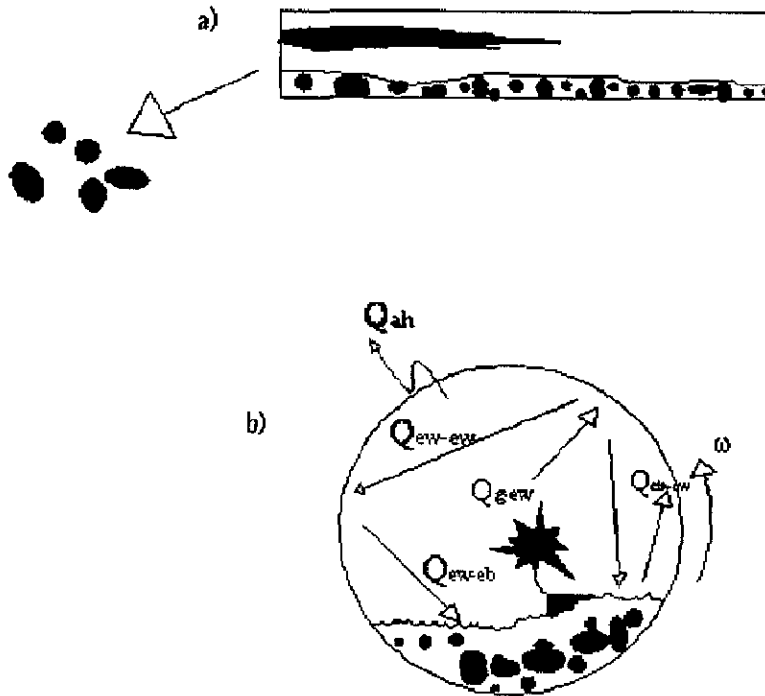


Figure 1.1: Schematic of Rotary Kiln (a) axial, and (b) cross-sectional

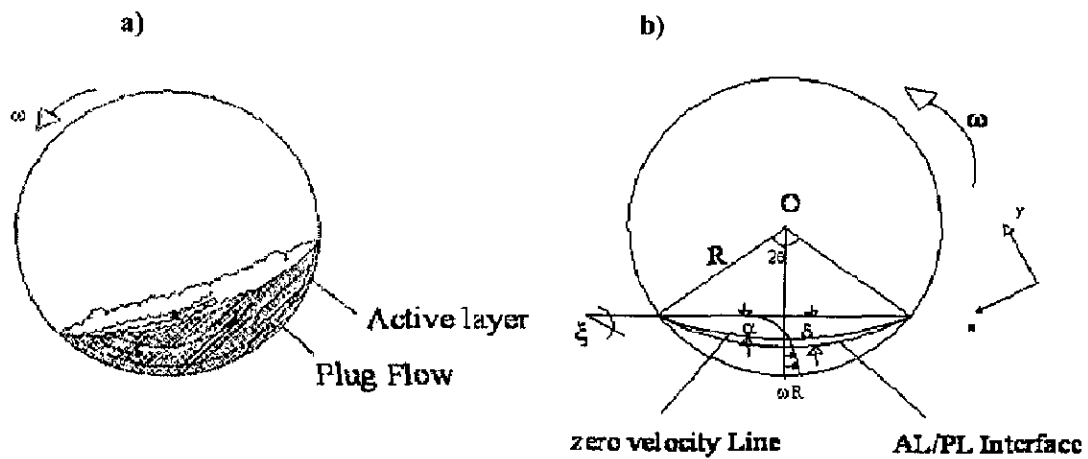


Figure 1.2: Granular flow in the transverse plane : (a) a rolling bed motion depicted two distinct region; (b) calculation domain for a rolling bed

Thus energy imparted by reactor's rotation is continuously fed into the plug flow region as potential energy which is subsequently released and dissipated in the active layer. The active layer itself is characterized by vigorous mixing and hence a high rate of surface renewal which promotes heat transfer from the freeboard. The vigorous particle motion may also promote de-mixing, termed segregation, in which smaller particles tend to sieve downward through the matrix of large particles. During segregation the bed motion tends to concentrate finer material within the core, and material within the core, because it has very little chance to reaching the exposed bed surface for direct heat transfer from the freeboard, tends to a lower temperature than the surrounding material. Thus, segregation tends to counter advective transport of energy and promotes temperature gradient within the bed. The net effect is not necessarily negative, for example in limestone calcinations smaller particles react faster than larger ones (at the same temperature) and therefore the segregation of fines to the cooler core may be obtaining uniform calcinations of all particles. This suggests that particle size distribution in the feed material might be optimized, which again points out the need for developing our predictive capabilities for the bed material.

## **1.1 BED BEHAVIOUR IN ROTARY REACTOR**








The motion of bed of particles in the transverse plane (perpendicular to the drum axis) as it moves from one end of the drum to the other can be characterized as one of the several possible behaviours. The behaviour depends on the operating condition (rotational speed and degree of fill) and the friction of the particles with each other and with the surface of the reactor wall. The different types of the transverse bed motion illustrated in table 1 in summary may be subdivided into three basic forms, namely slipping motion, cascading motion, and cataracting motion. To delimit the bed motion, the range for Froude's number and filling degree are specified, which, however, represent orientation values and are depends on the particular bed material used. The individual forms of motion are described as follows.



### 1.1.1 Slipping Motion

Under unfavorable frictional conditions between solid and cylinder wall ("smooth tube wall"), slipping motion can occur. There principally two types of slipping motion; sliding and surging. When the cylinder wall is very smooth *sliding* may be observed, which is characterized by a bed constantly sliding from the wall. The tube then rotates bed under the solid bed, the bed remaining as resting bed under a defined usually small angle of deflection. This form of motion ("standing state") can also occur at higher rotational speeds and filling degrees. With increasing wall friction, sliding turns into *surging*. This type of motion is characterized by periodic alternation between adhesive and kinetic friction of the bed on the wall. The solid bed adheres on the rotating wall up to a certain angle of deflection and subsequently slides back en masse on the wall surface. No particle mixing takes place in slipping motion. As a result, the product quality from rotary reactor decreases. Hence, this state of motion is undesired in practice and must be prevented through the utilization of rough wall or bars attached to the wall. Slipping motion, however, can not be avoided in every case and may occur at least partially in some product processes.

**Table 1 Different types of the transverse bed motion**

Basic form	Slipping motion		Cascading("tumbling") motion			Cataracting motion	
Subtype	Sliding	Surging	Slumping	Rolling	Cascading	Cataracting	Centrifuging
Schematic							
Physical process	Slipping		Mixing			Crushing	Centrifuging
Fraude's number [Fr]	$0 < Fr < 10^{-4}$		$10^{-5} < Fr < 10^{-3}$	$10^{-4} < Fr < 10^{-2}$	$10^{-3} < Fr < 10^{-1}$	$0.1 < Fr < 1$	$Fr \geq 1$
Filling degree $f$	$f < 0.1$	$f > 0.1$	$f < 0.1$	$f > 0.1$		$f > 0.2$	
Wall friction coeff. $\mu_w$	$\mu_w < \mu_{w,c}$	$\mu_w < \mu_{w,c}$	$\mu_w < \mu_{w,c}$			$\mu_w < \mu_{w,c}$	
Application	No use		Rotary kilns and reactors. Rotary dryer and coolers: mixing drums			Ball mills	No use

### 1.1.2 Cascading (Tumbling) Motion

Depending on rotational speed and particle size, the states of motion possible are *slumping, rolling and cascading*. When the rotational speed is low, slumping of the bed can occur. Through solid body rotation with the rotational speed of the cylinder wall, the solid bed is continuously elevated, being leveled off again and again by successive avalanches at the surface. The slumping frequency is dependent on rotational speed, particle size and cylinder diameter. Intermixing decreases as the filling degree increases to virtually at (degree of fill),  $f=0.5$ . As the rotational speed increases a flowing transition to rolling takes place, which is characterized by the uniform, static flow of the particle layer on the surface (cascading layer). The surface of the rolling bed is approximately flat and inclined at an angle (also known as the dynamic angle of repose,  $\theta$ ), which is determined predominantly by the inter-particle friction. This angle increases with increases the drum speed, and decreases with increasing particle size. The structure of the bed comprises of two layers; the active layer and the passive layer.

Within the passive layer, the bed is closed packed and the particles rotate with the drum at fixed radius and axial position. This is plug flow and there is little opportunity for particle interaction. Upon reaching the surface, particles roll downward and rejoin the passive layer. The active layer is dilated and the particles are in motion relative to each other and it is accepted that this is where all the mixing occurs. Radial mixing occurs as particles enter and leave the active layer at different radii. Axial mixing is attributed to deflection of particles by collision with other particles. The interface between the active and passive regions had been defined as the yield line surface. Above this surface, the particle is in active layer and moves in a direction predominantly parallel to the bed surface. Below the surface the particle rotates at the angular velocity of the drum. Velocity is continuous at the interface, hence the velocity of the particle at the interface is equal to the bed direction velocity component of the angular velocity in the passive layer and in negative direction (in opposite to bulk active flow). The turning point of the particle trajectory occurs above the interface, within the active layer.

As the rotational speed further increases, the bed surface begins to arch and cascading sets in. The transition to cascading is also dependent on particle size. The height of the arch of the kidney-shaped bed increases with rotational speed. The prevailing form of motion in a rotary reactor is cascading motion, provided undesired slipping motion can be prevented by creating sufficient wall friction conditions. Then in most cases the rolling bed is preferred, which provides favorable conditions for the heat transfer in high temperature processes and ensures a uniform, high quality of the product even when mass flow rates are high.

### **1.1.3 Cataracting Motion**

As rotational speed increases, the cascading motion is so strongly pronounced that individual particles detach from the bed and are thrown off into the free space of the cylinder. The release of particles is a characteristic feature of the cataracting motion, which may be subdivided into cataracting and centrifuging states of motion. Cataracting is characterized by particles from the bed being flung into the gas space. With rotational speed, the number of particles thrown off and the length of the trajectories increase until a uniform trickling veil forms along the diameter. In the case of further increase in the rotational speed, particles on the outer path begin to adhere to the wall and the extreme case of cataracting motion, centrifuging, occurs. Theoretically centrifuging reaches its final stage when the entire solid material is in contact with the cylinder wall as a uniform film. This stage is however only achieved, and only approximately as well, at extreme high rotational speeds. This form of motion is, however, not relevant for a rotary reactor, so that a further subdivision is refrained from.

## **1.2 DESIGN OF ROTARY REACTOR**

Most rotary reactors rotate around their axis which is inclined downward about  $2^{\circ}$ - $4^{\circ}$  from the horizontal. Their flow patterns are close to plug flow, such a flow pattern is often desired. However, sometimes it is not. In addition, the solids fraction in these

units are usually as small as 10%, while gas/solid contacting for the reaction is rather poor. Following are examples where some of these contacting difficulties may occur.

### **1.2.1 Thermal decomposition example**

Suppose a feed stream of manganese sulfate particle is to be heated to close to 1000° C. at an intermediate temperature; those solids liquefy, and then solidify at higher temperature to yield manganese oxide. When this operation is carried out in a conventional wall-heated rotary kiln, clusters of solids are apt to form at the reactor's wall and interfere with stable operations. This problem can be bypassed if we can mix fresh feed with product solids. This can be achieved by having recirculation in the rotary kiln or in critical section of the rotary kiln. However this is something which can not be done in a conventional rotary kiln.

### **1.2.2 Reactor example**

Consider activation of charcoal with the steam. Here particles are fed to the rotary reactor while steam has to diffuse through this large mass of moving solids. Kunii calculated the distribution of steam into layer of charcoal and found that hardly any steam penetrates as much as 3 cm in mass of solids. Since commercial rotary contactors are often are very large very thick layer of solids have to be penetrated by gas and this leads to diffusion problems which results in very poor performance compared with the ideal fluidized bed are ideal regarding the contacting of the gas with the particles; the solids are in mixed flow in a single unit, so to approach plug flow require multistage and that is not simple.

The above two examples shows that mixed flow of solid are desired in one case, plug in another. The novel design which we will describe here allows a great flexibility in contacting. For example, it will allow us to overcome the problem of cases are considered above.

### 1.2.3 Horizontal rotating cylinder with a partition plate and guide plates

Consider a horizontal rotating cylinder which contains a longitudinal partition plate and inclined guide plates on both sides of the partition plate as shown in Figure 1.3. Figure 1.4 shows the cross section of the cylinder, and Figure 1.5 shows what happens to a batch of solids as the cylinder makes one revolution. Note in Figure 1.5 (b) that the solids slide down on the surface of the partition plate. Since the guide plates are inclined, sliding plates are inclined; the sliding solids are displaced in axial direction. In Figure 1.5 (c) and (d) the solids tumble on the lower wall and drop into next section. In summary for each rotation of the cylinder the solids move from one section to next.

Let us look at the whole cylinder with guide plates and solids on both sides of the partition plates as shown in Figure 1.4. Rotating the cylinder has the solids on the both sides of partition plate moving from left to right. In contrast, consider the design shown in Figure 1.5 where the inclination of the guide plates is same on the both sides of partition plate. In this case rotation of the cylinder makes the solids on one side of the partition plate move from left to right, but from right to left on other side of the partition plate –thus yielding counter flow of solids. If the solids are allowed to cross from one side to other at the right end of the cylinder, the reactor behaves like plug flow unit twice as long as the shaft (see Figure 1.6(a)). Finally, if they partially cross over on the left hand end of the shaft then the solids recirculate, which in extreme gives mixed flow, as shown in Figure 1.6(b). In this arrangement a large circulation rate of solids can be achieved, so when feed stock is liable to stick or agglomerate, this flow pattern can usefully disperse feed within the circulating stream of solids.

### 1.2.4 Equation to estimate rate of solids movement

Consider the solids between two adjacent plates. In the ideal case when cylinder makes one rotation, solids will fall in to next section of the cylinder and will advance a distance.

$$\Delta l = d_t \cot \varphi \quad (1.11)$$

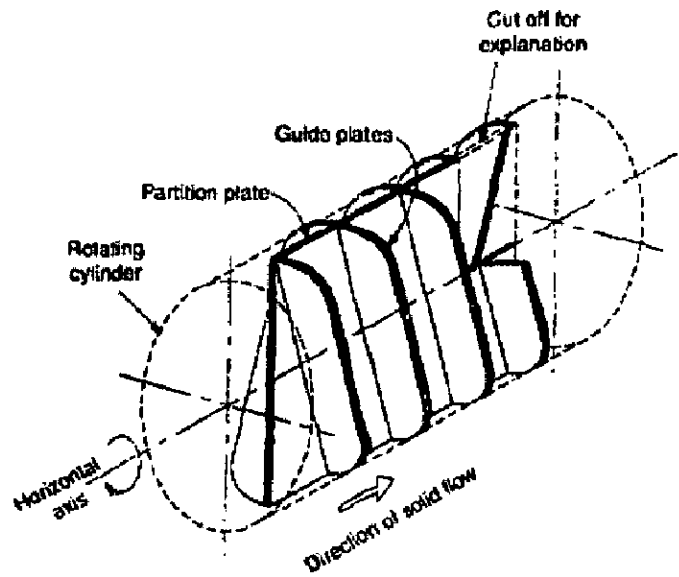


**Figure 1.3: Horizontal rotary gas/solid contactor for single movement**

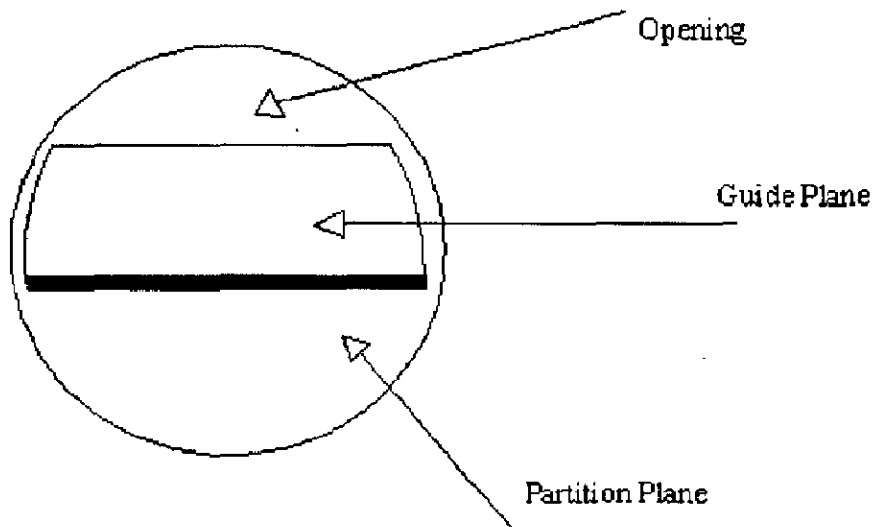


**Figure 1.4: Cross sectional of one side of the partition plate**

Where  $\varphi$  is the angle of inclination of the guide plates .If the slot opening or the dimensions of the guide plates is not right, then not the all solids will drop in the next section. We employ an efficiency of transfer of solids,  $\eta$  to deal with the above deviation.

Let the pertinent cross sectional area is of vessel:

$$A_t = \frac{\pi}{4} d_t^2 \quad (1.12)$$

From which the volume fraction of bulk solids in the vessel is

$$f_s = \frac{V_s}{V_t} = \frac{A_s}{A_t} \quad (1.13)$$

For side of the partition plate having one of the vessel cross-section, let the volume the solid which actually advance during one revolution of the cylinder be, from equation (1.11), (1.12) and (1.13)

$$V = \frac{1}{2} A_s \Delta l \eta = \frac{1}{2} \frac{\pi}{4} d_t^2 \Delta l f_s \eta = \frac{\pi}{8} d_t^3 \cot \varphi f_s \eta \quad (1.14)$$

With the steady rotation rate  $N$  (rev. per h) the flow rate of solids on each side of the partition plate is-

$$F_s = V \rho N = \frac{\pi}{8} d_t^3 \cot \varphi f_s \eta \rho N \text{ (kg / h)} \quad (1.15)$$

This gives internal circulation rate of the solids in a reactor such as that shown in Figure 1.4 Counting on both side of the partition plate, the total flow rate of solids is  $2F_s$ .

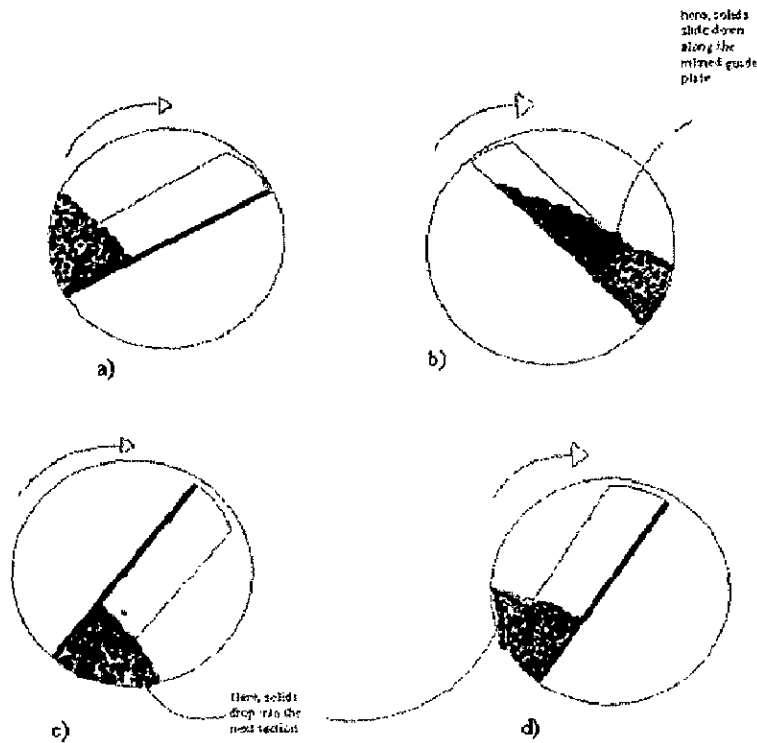


Figure 1.5: Movement of solid during one revolution of the cylinder (a) and(b): as the cylinder rotates the particle slide from one side to other , but do not pass through the guide plate;(c) and (d); here, particle tumble along the wall and drop into next section.

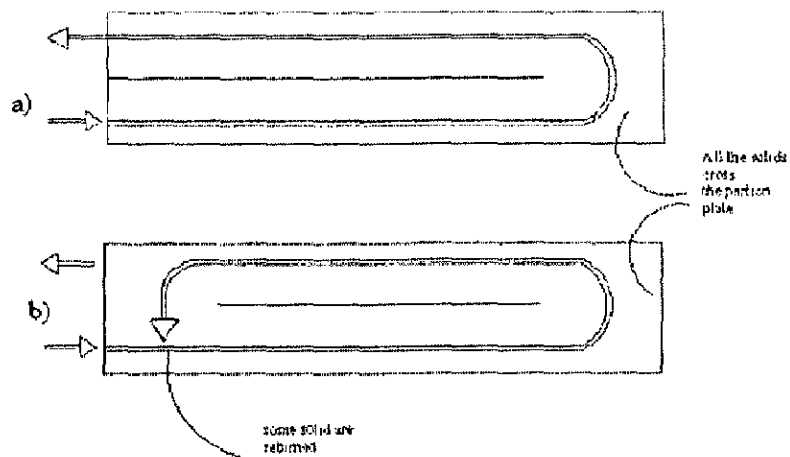


Figure1.6: Sketch showing how to achieve (a) a longer plug flow reactor and (b) an approach to mixed flow of solids



### 1.3 MODELLING OF ROTARY REACTOR (PREVIOUS WORK)

Rotary kiln has wide application in industry from the calcinations of limestone to cement manufacturing to calcining of petroleum coke etc. Problem such as low thermal efficiency and low product quality have plagued rotary kiln operation yet these machines have been survived and continuously improved over the century.

A series of equation representing conservation of mass energy and species averaged over cross section are solved using appropriate numerical methods. The critical assumption that must be made is that uniform conditions exist across the cross section in the free board gas, the wall/ refractories and bed. The bed for example is assumed to be well mixed and isothermal in any given transverse plane. Although these models have successfully been used in industry, they are limited in the amount of information that can be extracted. Flame positioning can be predicted in multidimensional model rather than used as an input.

In the most rotary kiln operations the chemical reaction in the bed require high temperature, for example, cement kiln require temperature approximately 1500°C. The energy to raise the temperature and drive endothermic reaction is from the combustion of range of fuels such as natural gas, coal and more and more alternative fuels. Heat transfer from gas to bed is complex and occurs from gas to the bed surface and kiln wall to bed surface through conduction, convection and radiation.

A number of rotary kiln models have been proposed over the years and recent computational fluid dynamics model can be developed but all have their limitations. In many cases it is not possible to measure gas flow rate at the kiln backend (gas exit) due to the configurations of ductwork. However, in most large kilns the backend O<sub>2</sub> is continuously measured along with temperature and pressure. Similarly at the kiln front end (product discharge) the kiln hood and cooler configuration make it impossible to measure the gas flow rate. Also at the end, the gas temperature is very difficult to

determine due to influence of radiation energy on measurement devices. The presence of backend gas analyzer makes the calculation of gas flow rate at this point simple to calculate if perfect combustion is assumed. The calculation of gas flow rate and temperature requires the solving of simultaneous equations.

Heat transfer at the interfacial surface is complex and involves radiation, convection and conduction. Although heat transfer rate at each slide can be calculated, it is extremely difficult to determine the realistic values. The conduction resistance is equal to  $\Delta x/kA$ , where  $\Delta x$  is the solid thickness,  $k$  is the thermal conductivity of the solid and  $A$  is the area. Convection resistance is equal to  $1/h_c A$  where  $h_c$  is over all heat transfer coefficient and  $A$  is the contact surface area. In series resistance are additive and in parallel their reciprocal are additive. The surface area used in the heat transfer equations are calculated as smooth surface, for example surface is assumed planar and is calculated from the volume of feed per segment.

A quasi-3D model developed comprises both an axial model (1D) and cross sectional model (2D). The former is used independently determine 1D axial temperature profiles for the freeboard gas and the bulk bed. Here it is assumed that the detail of energy distribution that occurs within the bed do not significantly heat transfer between the bed and freeboard. As part of the procedure for calculating these axial temperature profiles, the heat flux is determined and this becomes thermal boundary condition employed to drive the cross-section model. In doing so, bed temperature gradient computed from the axial model is used as sink term representing rate of removal to the material flow in axial direction. This dimensional bed is also employed as a checked on mass averaged temperature which is estimated from 2D bed model. The 2D model is consequently employed to determine the thermal condition of bed materials and the refractory wall over successive transverse section of the kiln.

Various models for rotary kiln have capability of predicting average conditions within both bed and freeboard as function of axial position. The thermal model of these

one-dimensional models can be derived by considering the transverse slice which divides the section into separate control volume of freeboard gas and bed material. Under steady state conditions, and in the absence of any chemical reactions or phase transformations, the energy conservation for any control volume requires that

$$\sum m_g c_{pg} \left( \frac{dT_g}{dz} \right) = Q_{g \rightarrow ew} + Q_{g \rightarrow eb} \quad (1.21)$$

$$\sum m_b c_{pb} \left( \frac{dT_b}{dz} \right) = Q_{g \rightarrow eb} + Q_{ew \rightarrow eb} + Q_{ew \rightarrow cb} \quad (1.22)$$

One additional condition which must be met is that no net energy accumulation can occur within wall which yields an auxiliary condition.

$$Q_{g \rightarrow ew} + Q_{eb \rightarrow ew} + Q_{cb \rightarrow cw} = Q_{shell} \quad (1.23)$$

The above system of equations can be solved for successive axial positions by a variety of techniques provided that heat transfer is characterized in terms of local gas, bed and wall temperature. Thus by starting at either end of the kiln, a complete solution of thermal problem can be developed. It is the major methodology employed in evaluating heat transfer terms which distinguishes various one-dimensional modes.

Heat transfer at interfacial position is complex and involves radiation, convection and at the covered bed-covered wall interfaces conduction as well. Although heat transfer coefficient can be allocated for each transport path shown in Figure 1.1 this should not obscure the difficulty associated with realistic determination of values for these coefficients. In the present work one-dimensional model is only required to produce a frame work for which to operate the 2D thermal model of the bed and therefore additional models were used to evaluate heat transfer at interfaces. It is required to take into account factors such as single particle heat transfer coefficient wall to bed radiation

solid to solid heat conduction, continuum heat conduction through the gas and gap between the bed and wall surface.

Since there should be no intent to restrict the work to the non reactive conditions in the bed and freeboard, Equations (1.21) and (1.22) may be transformed to include reactive terms to yield the following system of equations:

$$\sum m_{gi} c_{pgi} (dT_g/dz) = h_{ew} A_{ew} (T_g - T_w) + h_{eb} A_{eb} (T_g - T_w) + \sum \lambda_i A_g \Delta H_{rg} \quad (1.24)$$

$$\sum m_b c_{pb} (dT_b/dz) = h_{eb} A_{eb} (T_b - T_g) + h_{cw} A_{cw} (T_b - T_w) + \sum \lambda_i A_b \Delta H_{rb} \quad (1.25)$$

where  $\lambda$  is the production rate for various species involved in either chemical reaction, e.g. free board combustion, or phase changes each to be determined by the appropriate kinetic expressions.

### 1.3.1 The two dimensional thermal model applied to the bed

Although useful results have been obtained from 1D model, the assumption that conditions will be uniform over any transverse section of the bed material will hold for mixed bed. Since segregation is known to occur within the bed, a 2D model provides an opportunity to examine the effects, on kiln performance, of mixing within the bed. Such conditions are driven by bed motion which is in turn established by kiln rotation. However, because no adequate model for this motion has previously been reported, attempts to predict conditions within the 2D or 3D are rare.

It was mentioned earlier that rolling bed mode, which is preferred in most kiln operations, comprises two distinct regions. Because of improved mixing during rolling, it

is considered as mode of operation for thermal model. In this model heat transfer occurs within the active layer by conduction and convection. Since flow within the active layer is primarily parallel to the top surface, Cartesian system was attached to this region for heat transfer calculations. In order to simplify the analysis, the bed was assumed to consist of simple inert component and behave as a continuum. Energy conservation for a control volume in the active layers require that

$$\frac{\partial}{\partial x} \left( k_{ef} \frac{\partial T}{\partial x} \right) - \rho_p u_x \frac{\partial T}{\partial x} + \frac{\partial}{\partial y} \left( k_{ef} \frac{\partial T}{\partial y} \right) - \rho_p u_y \frac{\partial T}{\partial y} + m_{fx} c_{pb} \frac{dT_{ba}}{dz} = 0 \quad (1.26)$$

It is further assumed that mixing is sufficient to ensure that, within the active layer, the temperature gradient in the axial direction of the kiln is uniform. Since, for every kiln rotation the bed material makes three to four excursions in the transverse plan, mixing is more as compared to that in axial direction. Hence, the last term in Equation (1.26), which includes axial gradient of temperature in the active layer accounts advance axially at the same rate and because plug flow region behaves as a rigid body, this axial advance occurs only within the active layer. In order to solve Equation (1.26), the convective term as well as mixing effects on  $k_{ef}$  must be determined by an adequate granular flow model.

In contrast to the active layer, the plug flow region is relatively deep and since it rotates as a rigid body about the kiln axis, a cylindrical coordinate system was applied to this region as well as to refractory wall itself. Energy conservation for any control volume in the plug flow region and the wall requires that

$$\frac{\partial}{r \partial r} \left( k_{pf} r \frac{\partial T}{\partial r} \right) + \frac{1}{r^2} \frac{\partial}{\partial \theta} \left( k_{pf} \frac{\partial T}{\partial \theta} \right) - \rho_{pf} C_{p_{pf}} \omega r \frac{\partial T}{r \partial \theta} = 0 \quad (1.27)$$

$$\frac{\partial}{r \partial r} \left( k_w r \frac{\partial T}{\partial r} \right) + \frac{1}{r^2} \frac{\partial}{\partial \theta} \left( k_w \frac{\partial T}{\partial \theta} \right) - \rho_w C_{p_w} \omega r \frac{\partial T}{r \partial \theta} = 0 \quad (1.28)$$

where the first two terms consist of radial and transverse conduction respectively and the third term represents the movement of energy through the control volume due the rotation of the kiln.

**LITERATURE REVIEW**

---



---

In this chapter, the CFD model and the mathematical model describing the heat and mass transfer phenomena in the rotary reactor by various research workers have been discussed with respect to their objectives, assumptions, solution methodology and pertinent conclusions.

**2.1 Gorog *et al.*(1982)**

The authors have developed a mathematical model of the rotary kiln to determine the temperature distribution in the wall of the rotary kiln by incorporating radiative and convective heat transfer coefficient in a kiln in the model. The focus of the study was on the development of a mathematical model to predict the temperature field in the kiln wall, and determination of heat transfer coefficient. The conductive heat transfer, based on constant thermo-physical properties of the wall, negligible heat conduction in the longitudinal direction as well as by the circumference, was governed by the following equation:

$$\frac{\partial(k_w \frac{\partial T_w}{\partial r})}{\partial r} + \frac{k_w}{r} \frac{\partial T_w}{\partial r} + \frac{1}{r^2} \frac{\partial}{\partial \phi} (k_w \frac{\partial T_w}{\partial \phi}) + \frac{\partial}{\partial z} (k_w \frac{\partial T_w}{\partial z}) = \rho_w C_{pw} \frac{\partial T_w}{\partial t}$$

It was observed that for the calcinations zone the circumferential inner wall temperature varied by 55K with an active layer thickness of 9 mm. The amplitude of temperature cycles at the inner wall was directly proportional gas temperature and the difference between the gas and solid temperature. A sanky diagram had been constructed for each zone which show relative amount of energy transferred to the solid directly from the freeboard and indirectly by the regenerative action of the wall was a function of the kiln position. Heat transfer to the solid in high temperature region 60-80% were

contributed by radiation and in low temperature region 70% of heat were contributed by freeboard convection and the regenerative heating of the wall.

## **2.2 Chakrabarti (2002)**

### **Investigations on heat loss through the kiln shell in magnesite dead burning process: a case study**

This study investigated the heat losses from rotary kiln through radiation and convection in the process of burning of magnesite ore. In calculating the heat losses, the heat loss through radiations; force and free air convection were taken into account. It was concluded that heat losses through the first 30 meters contributed 49 % of heat loss by the shell of kiln.

## **2.3 Meier *et al* (2004)**

### **Design and experimental investigation of a horizontal rotary reactor for the solar thermal production of lime**

A 10 kW horizontal rotary reactor was designed and tested for production of lime from calcium carbonate. In contrast to the conventional tilted cylindrical rotary reactor, the designed reactor had a conical reaction chamber with a fixed cone angle of 5°. The solar lime reactor worked in continuous mode and raw material was stored in a hopper that was placed on top of the rear part of the reactor. The residence time of the reactant inside the reaction chamber was controlled by adjustment of the feed rate and the rotational speed. The efficiency of the reactor, defined as the rate of heat required for the enthalpy change of the calcinations reaction at specified temperature to the solar power input, was about 13 % while maximum efficiency reached 20%. It has been claimed that efficiency could be theoretically improved to 83 % by recovering the thermal energy from the product and by reduction in conduction heat loss, and convected heat loss as the gaseous product exits the reactor.



## 2.4 Martins *et al.* (2001)

### Modelling and simulation of petroleum coke calcination in rotary kilns

A one dimensional model was developed for the simulation of petroleum coke in the rotary kiln to manufacture carbon electrode. The green petroleum coke was calcined to remove moisture and volatile matter. The model comprised of 14 ODEs based on mass and energy balances. Heat transfer by conduction, convection and radiation were taken into account. Mass transfer occurring between the solid and gaseous phase were attributed to volatile component combustion reaction. The authors considered the variation of all physical, chemical and rheological properties along the bed. Heat fluxes were calculated by empirical correlations specific for rotary reactor. They considered radiation heat transfer between the gas phase and the bed, between the gas phase and the kiln internal wall.

$$Q_{rgk} = \sigma A_{rgk} (\epsilon_k + 1) \left( \frac{\epsilon_g T_g^4 - \alpha_k T_k^4}{2} \right), k = s, w \quad (2.11)$$

The kinetics of release of coke particles to the gas phase was described by empirical correlation in which gas temperature, gas density, radius of particles were incorporated. The temperature profiles of the solid bed showed a little depression in temperature at 5 m from the solid feed end, due to the injection of tertiary air at that point and rise in temperature of bed upto 40m. The temperature profile of the solid bed and for the composition of the gas phase presented better agreements with measured industrial data.

## 2.5 Ortiz (2005)

### Dynamic simulation of pilot rotary kiln for charcoal activation

Rotary kiln was used to manufacture the activated carbon from charcoal with water vapor. The dynamic simulation system was developed using Simulink-Matlab

framework to understand the behavior of the reactor. The three transient operation modes simulated were start up, shut down and no steady-state operation due to disturbances in the manipulated variable. The model equations were obtained by the regression analysis from laboratory test with a discontinuous reactor. It was assumed that both solid and gaseous axial velocity changes were negligible, all variables were uniform in the radial direction, no gas or solid axial mixing, regenerative effect of the wall was negligible. The water flow rate was constant and physical properties were constant and independent of temperature. The residence time has been used in that work was

$$t = \frac{0.19L}{ND_i S} \quad (2.12)$$

The calculation results for the start up period gave relevant information about the time required to reach a constant temperature in the bulk of the gas and about the most adequate feed gas temperature. The disturbance analysis gave information about the dynamic open-loop response of the system due to step changes in the main input variables of the process. The simulated response, however, agrees with the actual rotary kiln behavior in the retention (dead) time.

The simulation of the shut-down operation mode shows that the process requires approximately 1.5 h to cool down it. This time must be considered before turning off the rotation device in order to prevent breaking in the refractory bricks. The necessary time to empty the solid from the rotary kiln is around 2 h. The diary operation plan must include both time intervals.

## **2.6 Ortiz *et al* (2003)**

### **Steady state simulation of rotary kiln for charcoal activation**

The mass transfer due to the chemical reaction was modelled using a simple kinetic equation generated from author's experimental data, which allowed the simulation of the mass transfer between solid and gas. The relative importance of the heat

transferred by radiation with respect to other transfer phenomena was also verified since the model was particularly influenced by changes in those coefficients. The results obtained from the steady state simulation exhibited the effects of the heat and mass transfer, when the activation reaction was carried out. The comparison with characteristic experimental values from the literature was reasonably good which occurred in spite of the model middle complexity and neglect of the regenerative effect of the wall. The model, once improved with their experimental data, will permit the adaptation of the operation conditions of the rotary kiln to reduce the energy consumption and to improve product quality.

## **2.7 Kim and Srivastava (1988)**

### **Simulation of an industrial Rotary Calciner with trona ore decomposition**

The objective of this research was to simulate the steady state operations of a commercial scale calciner with the trona ore decomposition. The 27 m reactor used was divided into three sections: first section of 6 m length contained no lifter to provide sufficient length to minimize showered of solids through the flame, the second section of 18 m contained lifters while the third section of 3 m which allowed the dust disengagement from the gas. Mass, component and energy balances for endothermic decomposition of material ore (Sodium Sesquicarbonate) into soda ash resulted into non-linear differential equation and algebraic equations which were intercoupled. It was suggested that retention time of solid in a rotary cylinder shell was a function of diameter, length, slope and rate of revolution of shell and physical characteristics of the solids. In the flight fitted section the retention was strongly dependent upon the dynamics of the particle movement in the gas stream. The simulated results showed that a sharp variation in the profile at 6 m from the feed end of the calciner was due to lifter which also responsible for increased in heat transfer rate. The solid temperature rose sharply until a point was reached where the rate of endothermic reaction balance the heat transfer rate from the hot gas stream.

## 2.8 Van Dijen and Metselaar (1989)

### Chemical reaction engineering aspects of a rotary reactor for carbothermal synthesis of SiC

In this paper, SiC powder production on small scale from SiO<sub>2</sub> and C in rotary reactor has been described. The first reaction was a direct solid state reaction whereas the second consisted of solid state reaction followed by a gas- solid reaction. A rotary reactor with a graphite tube and graphite heating element outside the tube were used in the experiments. The displacement of material in the longitudinal direction was described by the following equation:

$$t = \frac{KL}{ND \tan \alpha} \quad (2.13)$$

where, L is the length of the heated zone

N, rotational speed in rpm

$\alpha$  , the angle of inclination

K, factor dependent upon degree of filling

The heat was transferred from the heating element to the tube, through the tube and from the tube to the bed and the heat which was transferred from the heating element to the bed was entirely used to heat up the particles. Radiation heat transfer dominated over conduction and convection from the heating element from the tube. The experiments showed that the carbothermal reaction runs smoothly at 20% degree of fill and a reaction time of 30 minutes. It was observed that with the increase of degree of fill, decrease in the residence time will result. The temperature difference between the heating element and the bed increased proportional to the tube diameter.

## **2.9 Palmer (1998)**

### **Heat transfer in rotary kiln**

The aim of this paper was to understand heat transfer in rotary kiln and to provide a systematic basis for the efficient design of kiln. The kiln models were developed on general mass and energy balance over the process. The proposed heat transfer model consists of thermal resistances from the gas to wall, gas to bed surface, wall to bed surface, bed surface to bed centre, bed centre to wall and from wall to atmosphere as shown in figure. During the experiments, it was assumed that combustion of fuel began at 2 m inside the kiln and completed at 32m into the kiln. The energy released profile followed a parabolic function. It was observed that the average bed temperature enhanced as the material moved along the kiln in the axial direction. The model was validated with the experimental data.

## **2.10 Boateng and Barr (1996)**

### **A thermal model for the rotary kiln including heat transfer within the bed**

A mathematical model was developed to predict heat transfer from the freeboard gas to the bed of rotary kiln and examined the role of bed motion in the transverse plane in determination of energy distribution within the bed. A 2-D cross sectional model as well as 1-D axial model was developed for thermal and flow behaviour. These two separate models were combined to give a quasi 3-D model for the bed material. The kiln operates under counter current operation. The model was validated with the experiment which consisted of two parts. For mixed bed conditions, typically a rolling bed with uniform particle size, the velocity field that results from kiln rotation, as well as self-diffusion, enhanced the effective thermal conductivity of the bed and promoted temperature uniformity. The temperature gradients within the bed, for a moderate fill of 12% Ottawa sand in the pilot kiln, at all local freeboard gas temperatures (600-1200°C),

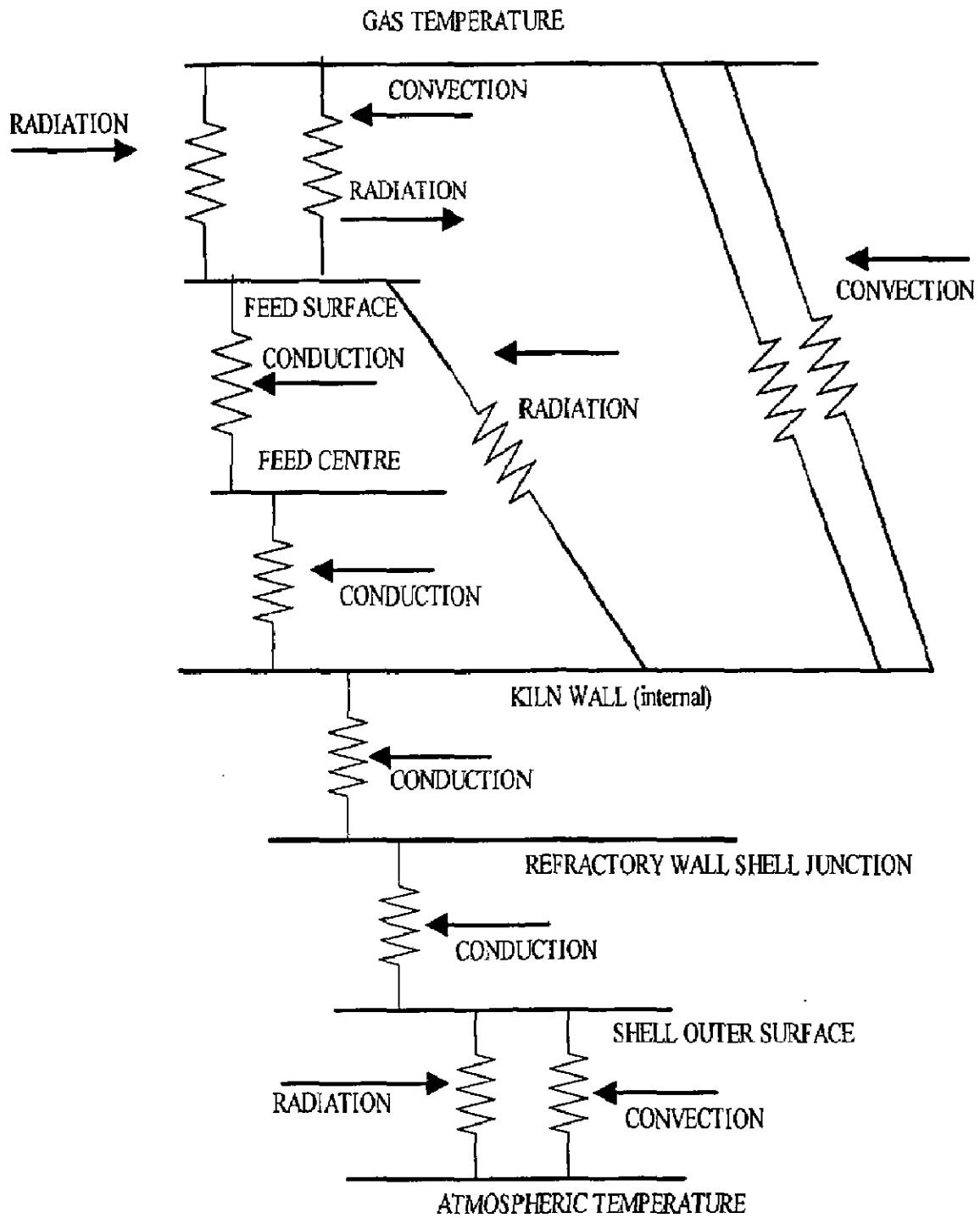


**Figure 2.1: Thermal Resistance Model**

do not exceed 30°C for lower rotation rate (typically 1.5 rpm for pilot kilns). Because of strong diffusion effects due to improved granular flow behavior, the bed tends to isothermal conditions at higher kiln rotation rates. For a segregated bed, which was the condition with marked particle size differences, and also for a condition whereby the flow field suppresses radial diffusion (e.g. slumping bed mode), temperature non-uniformities existed within the bed. The introduction of 20% fines into the charge for a pilot kiln at the same operating conditions as a mixed bed might result in bed surface-to-core temperature difference of over 200 °C, with the cooler region coinciding with the segregated core.

### **2.11 Sheritt *et al* (2003)**

#### **Axial dispersion in the three dimensional mixing of particles in the rotating drum reactor**

In this paper new design equations were proposed for the axial dispersion coefficient in terms of rotational speed, degree of fill, drum diameter and particle diameter. The validation of the model equations was achieved with 179 data points from both batch and continuous mode. During the experiments, single radioactive particle tracking technique was employed to confirm the proposed design correlations and a horizontal drum of 200 mm diameter and 900 mm length was used which contained a bed of uniform 3mm diameter spherical glass beads. Sodium iodide scintillation detectors were used to detect the tracking of single radioactive particle in the multi phase fluidized bed. Nuclear decay of tracer particles emitted gamma rays that were detected by the scintillation detectors. The proposed correlation included diameter of particle, degree of fill, diameter of drum and rotational speed and the correlation was derived by data regression and tested for significance (F-test). Mixing in axial direction was purely diffusive and was caused by random collisions of particles in the active region. Axial mixing was described by one dimensional diffusional equation. The coefficient was proportional to the drum diameter for all type of bed behaviour and proportional to square root of particle diameter. For rolling and cascading bed behaviour the coefficient was

proportional to the square root of speed and increased proportionally with the drum diameter keeping all other variables constant.

### **2.12 Santomaso *et al* (2005)**

#### **Mixing kinetics of granular material in drums operated in rolling and cataracting regime**

This investigation is concerned with the comparison of mixing efficiency of two regimes i.e. rolling and cataracting. It was seen that a proper combination of two regimes achieves better mixing quality more rapidly. The internal of the bed had been investigated through a solidification technique. In the experiments, tetraacetyldiamine powder in blue and white was used. In a horizontally positioned drum at a controlled speed drum with length to diameter ratio equal to 1.18 had been adopted. The bed had been impregnated with molten wax and then solidified and sliced perpendicular to the cylindrical axis. To quantify the axial concentration distribution, each section had been averaged. Two experiments of 1600 and 1200 revolutions were performed for rolling and cataracting design respectively and the result were plotted in terms of variance versus number of revolutions. It was observed that after 200 revolutions mixing in the axial direction was enhanced mainly at the end by a higher rotational speed. It was observed that cataracting attains higher mixture homogeneity. Moreover, with less revolution cataracting achieved better results in terms of axial homogeneity. An increase in the rotational speed from the rolling to the cataracting design could increase the mixing efficiency in terms of mixture uniformity and mixing rate. The result of the experiment carried out in the cataracting design fitted well in the diffusive model



### 2.13 Mellmann (2001)

#### The transverse motion of solids in the rotating cylinders- forms of motion and transition behaviour.

This study deals with the development of mathematical models to predict the transition between the different forms of transverse motion in unbaffled rotating cylinder. Criteria equation was derived from the model in form of critical wall friction coefficient and critical Froude's number as a function of filling degree. The transverse motion behaviour of granular solid in rotating cylinder was represented on bed behaviour diagram. The transition between the slipping motion and cascading was calculated as

$$\mu_{w,c} = \frac{2 \sin^3 \varepsilon \sin \phi}{3\pi f (1 + Fr)} \quad (2.14)$$

where,

$\varepsilon$  is half bed angle of the circular segment occupied with solid's,

$f$  is filling degree,

$\phi$  is the dynamic angle of repose,

Fr is Froude number

The flow ability of the solid walls is related to dynamic angle of repose. The transition from cascading to cataracting motion with low filled degree was to be expected only at very high rotational speed.

### 2.14 Li *et al.* (2002)

#### Axial transport and residence time of MSW in rotary kilns: Part II. theoretical and optimal analyses

In this study, a novel particulate trajectory model (PTM) was developed to predict axial transport and dispersion of municipal solid wastes, based on the vector analyses on the gravity – induced axial displacement of particle in a single excursion. This work can

be categorized into three sections with respect to PTM. First, the empirical formulae on both mean residence time (MRT) and material volumetric flow (MVF) had been deduced by employing the statistical-averaged analyses on all rolling steps of particles into PTM. It is assumed that the rolling of particles in the active layer is induced only by the gravity. The authors have proposed the inclusion of two correctional factors – one each for MRT and MVF – to improve model's applicability under practical condition. Good agreement had been obtained between the empirical formulae and experiments with correlation factor in excess of 90 % in all runs.

Secondly, a stochastic PTM is extended to predict the RTD curves of segregated MSW by considering the probability of the rolling distance of individual particle. The main purpose of random PTM is to introduce the certain number of tracers into a steady-state rotary kiln, calculate the residence time of individual tracer one by one and conduct the statistic analysis on the distribution of all tracers. The main cause of the dispersion of RTD is the segregation of particle rolling distance in a single excursion, due to variation of MSW flow properties. The simulated RTD from stochastic PTM fits quite well with the experimental one while the model equation predicts a slightly shorter MRT than experiments.

Finally, the optimizing model for the geometry design of a laboratory – scale rotary kiln pyrolyser had been proposed and the optimal solutions discussed by the authors which may provide insight in the design and development of a technical – scale rotary kiln pyrolyser of waste tyre.

### **2.15 Marias (2003)**

#### **A model of a rotary kiln incinerator including processes occurring within the solid and the gaseous phases**

This study is concerned with the modeling of the burning bed or gaseous turbulence combustion and subsequent radiation. It is based on the coupling of a

simplified model for the burning bed and the standard models of the CFD tool (*Fluent*). In this study, a balance approach (chemical element and energy) has been used to characterize the composition of the gas. The model for the bed has been introduced in the software *gPROMS* and this part shows some typical results, given the kiln geometry and the operating conditions of the furnace.

The CFD model incorporates all the relevant physical phenomena occurring within the gaseous phase including turbulence, chemical species transport and reaction and heat transfer. Turbulence modeling was achieved by using the two-equation  $\kappa - \epsilon$  model, which permits the computation of the turbulent viscosity and thus the Reynolds stress tensor.

The coupling of the modeling and CFD tools has been achieved by using boundary condition. The mass flux of volatile matter predicted was one-dimensional because the bed model is only one-dimensional. However, because the CFD model was fully three dimensional, it required a two dimensional profile which was achieved by interpolation and extrapolation in order to share data.

The developed model was able to predict the combustion of the volatile matter within the incinerator as well as the subsequent radiation received by its walls, and the thermal and chemical species contours.

## **2.16 Sofialidis *et al* (2005)**

### **Modelling low-temperature carbonisation of solid fuels in a heated rotary kiln for clean fuel production**

This work deals with the numerical simulation of the physico-chemical processes occurring inside a heated rotary kiln reactor, where coal, lignite or biomass are treated in

vacuum for the production of clean solid fuel, has been performed with FLUENT6 Computational Fluid Dynamics (CFD) code. The authors proposed a compact and reliable procedure for the prediction of solid fuel carbonization. The model formulation strategy includes two steps: (a) cold – flow simulations, which provide the confirmation of an industrial – scale kiln design able to offer an adequate residence time, and (b) full ‘hot’ runs.

This study simulated the dense, reacting gas-solid flow in an Eulerian network which includes the detailed modelling of all coal particle processes, including particle drag, turbulent dispersion, heat-up, drying, volatilization, pyrolysis and heterogeneous gasification. The coal particles were characterized by the content in raw coal, ash, moisture and char. The proposed model solves for the heterogeneous reactions between gaseous and solid species which was incorporated in the Eulerian multiphase network code, appropriately customized to incorporate the unique features of the proposed model.

#### **2.17 Watkinson and Brimacombe (1982)**

##### **Limestone calcination in a rotary kiln**

The author in this paper described the important operating variables on the heat transfer and calcinations process of limestone in the pilot rotary kiln. An experimental study of limestone calcinations for 5 different types of limestone was carried out and it was observed that temperature decrement followed nearly linear fashion from the burner zone until the charge end. The calcination processes were completed within 1350 K for each limestone which followed S-shaped curve of gas temperature profile independent of operating conditions. The percent calcination was found to be decreasing inversely with the feed rate. The solid temperature increased nearly linear along the kiln. The effect of kiln inclination showed that steepest angle resulted in poor mode of operation. The smallest inclination corresponds to greatest yield of calcinations.

## **2.18 Dumont and Belanger (1978)**

### **Steady state study of titanium dioxide rotary kiln**

The operation of rotary kiln for titanium dioxide was described in this study by employing mathematical models based on mass and energy balances. The mathematical models were solved by implicit method coupled with Newton-Raphson algorithm. The agreement of models was seen to be reasonable with the experimental results. It was suggested that there exist a substantial potential to improve the economy of the kiln operation.

## **2.19 Manitius *et al.***

### **Mathematical model of aluminum oxide rotary kiln**

This paper describes the mathematical model of rotary kiln for the calcinations of aluminum sulphate in the production of aluminum oxide. The models were derived from mass and energy balances, consisting of 22 ODEs. Spiral type motion of the particles in the rotary kiln as a function of pouring angle, kiln inclination and inner diameter of the kiln was assumed during this study. These models were solved in ALGOL programming. The computed results showed the temperature of material rose slowly in the reaction zone of the reactor. It was observed that theoretically 72% of the heat received by the material from both gas and wall was consumed by chemical reactions. The simulation results, matched reasonably well with the experimental values which could be further improved by narrowing the uncertainty margin in parameter values.

## **2.20 Wes *et al.* (1976)**

### **Heat Transfer in a horizontal rotary drum reactor**

The aim of this paper was to understand the heat transfer and to derive the heat transfer coefficient. An industrial scale rotary reactor of 9m in length and 3m in diameter was used in the experiments which were performed on potato starch and yellow dextrine. The penetration model in PDEs form was considered which could better describe the heat

transfer between wall and solids. The heat transfer coefficient was then defined in terms of thermal conductivity, density, heat capacity and time. It was concluded that at constant degree of fill the heat transfer coefficient was proportional to square root of the rotational speed.

## MODELLING OF ROTARY REACTOR

---

---

The activation of charcoal and calcination of limestone in Rotary Reactor have been described by means of model equations based on mass and energy conservation. Heat transfer by conduction, convection and radiation between solid gas and wall is taken into account. Mass transfer occurring between the solid and gas phases is mainly due to release of carbon dioxide in the reaction. The model equations were validated on two different solids, limestone and wood for different conditions whose experimental results were available in Ortiz *et al.* (2003a) and Barr *et al.* (1989). Figure (3.1) presents the control volume used to develop the model, representing the reactor cross-section with respect to the axial ( $z$ ) direction. Each dependent variable is represented by the average value in the reactor cross-sectional.

In order to model the transfer phenomena for the existing phases, the differential mass and energy balances, which include chemical reaction terms, are presented in cylindrical coordinates. The following assumptions were used during this study:

- Solid as well as gas linear velocity changes are negligible.
- All variables are uniform in the radial direction due to small size of reactor.
- There is neither solid nor gas axial mixing. The two phases are in plug flow. Solid drag by gas is negligible.
- Variations in rotary reactor wall temperature in the angular direction are negligible.
- Constant steam flow rate.
- Pressure of the reactor is constant.
- Axial heat transfer by conduction and radiation is negligible.
- Axial heat transfer by conduction inside the wall is not considered.
- Heat of reaction is supposed to be constant and independent of temperature.
- Regenerative effect of the reactor is neglected.

### 3.1 CHEMICAL REACTION KINETICS

#### Case I) Charcoal Activation

Solid disappearance is a consequence of the chemical reaction between carbonaceous material and steam. The reaction is as follows



Rate of decomposition of carbonaceous material is given as [Ortiz *et. al.* 2003a]

$$\gamma_s = -\frac{\partial Q_s}{\partial z} = 6.005 \exp\left(\frac{-8033}{T_s}\right) \frac{Q_a Q_s}{V_s} \quad (3.11)$$

The secondary reaction which is the formation of CO<sub>2</sub> from CO and steam is called as Water Gas Shift Reaction (WGSR).



Rate of disappearance of CO is given by [Sato *et al.* 2004]

$$\gamma_{co} = -\frac{\partial \text{CO}}{\partial t} = 10^{12.7} \exp(-2.83 \cdot 10^5 / RT) [\text{CO}]^{0.5} \quad (3.12)$$

Primary reaction is occurring at 1073 K that leads to the formation of CO and which drives the secondary reaction. The water gas shift reaction is very fast and endothermic at this temperature. The net effect of this reaction is an increase in energy of the gas while the products of WGSR are also in gaseous state which means that mass of gas remains the same and independent of this reaction.



## Case II) Calcinations of limestone

The chemical reaction of limestone thermal decomposition is described as follows;



The heat of reaction ( $\Delta H_R$  at  $600^\circ\text{C}$ ) is 1.7 MJ/kg of  $\text{CaCO}_3$ . The limestone decomposition reaction is endothermic. The reaction occurs in the decomposition zone of the rotary reactor (second zone) due to the large heat transfer from the gas phase (hot gases) to the limestone granule surface (solid phase).

The limestone when introduced on the upper side of the reactor is heated by the gaseous phase up to the thermal decomposition temperature ( $\sim 600^\circ\text{C}$ ). On the upper side of the reactor, the gaseous stream, rich in carbon dioxide, is evacuated. In the second zone of the reactor the decomposition of limestone is performed at a temperature between  $600 - 1200^\circ\text{C}$ . The lime resulting in the decomposition zone is evacuated after the third zone where the gaseous phase introduced at the lower end of the reactor. The lime product and the residual limestone are evacuated at this end. The disappearance of limestone is given by [Luisser, 2004]:

$$\frac{\partial x_{\text{CaCO}_3}}{\partial t} = 98000 \exp\left(\frac{-142000}{RT}\right) \sqrt{1 - x_{\text{CaCO}_3}} \quad (3.22)$$

### 3.2 MODEL DEVELOPMENT

Consider the reactor scheme shown in figure (3.1). The raw materials are comprised of solids which may be wood particles or lime stone particle. Hot gases liberated from the combustion of methane supplies the necessary heat of the reaction. Gas is moving counter-currently with the solid. The model equations are derived based on mass balances on the moisture contained in the solid and gas, while energy balances have been obtained from the solid, gas and wall of the reactor. The solid particle rolls in the reactor as the reactor rotates. The motion of the particles in the axial direction of the reactor is taken as positive and represented by  $z$ . Consider a control volume of thickness  $\Delta z$  at a distance of  $z$  from solid input end of the reactor as shown in figure (3.1).

#### 3.2.1 Mass balance of moisture into the control volume

- Rate of flow of moisture into the control volume =  $Q_h|_z$
- Rate of flow of moisture out from control volume =  $Q_h|_{z+\Delta z}$
- Rate of consumption of moisture proportional to the moisture content =  $k_h Q_h \Delta z$
- Rate of accumulation of moisture =  $\frac{\Delta}{\Delta t} \left[ Q_h \cdot \frac{\Delta z}{v_s} \right]$

where,  $v_s$  is solid velocity

Applying the balance

$$\frac{\Delta}{\Delta t} \left[ Q_h \cdot \frac{\Delta z}{v_s} \right] = -(Q_h|_{z+\Delta z} - Q_h|_z) - k_h Q_h \Delta z$$

Dividing the above equation by  $\Delta z$  and taking the limit  $\Delta z \rightarrow 0$  and  $\Delta t \rightarrow 0$

$$\frac{1}{v_s} \frac{\partial}{\partial t} Q_h = - \frac{\partial}{\partial z} Q_h - k_h Q_h$$

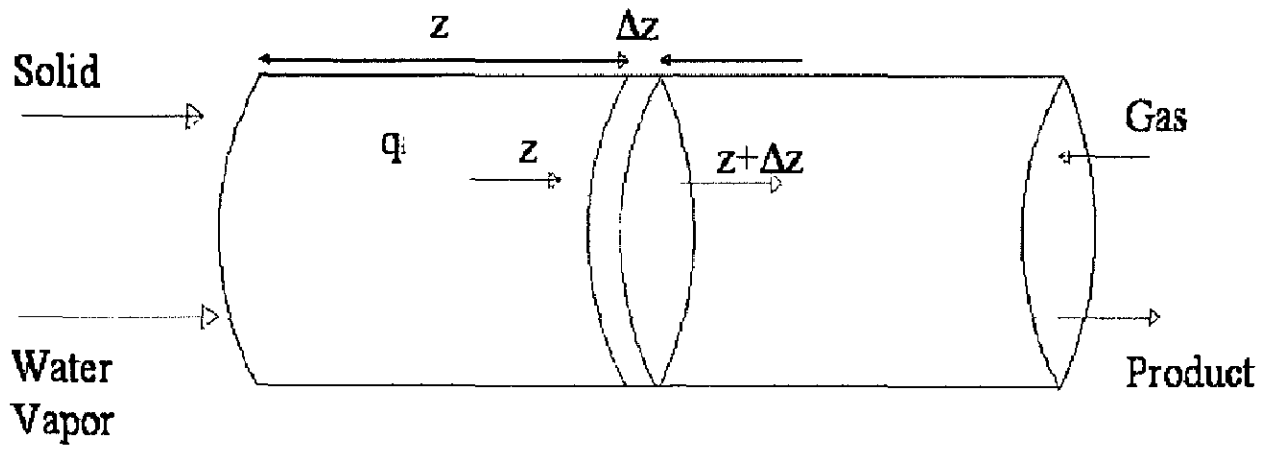


Figure 3.1 Reactor scheme

$k_h$  is the constant determined at the boundary between the two drying periods, which occurs when the moisture content of the solids equals the critical moisture content . Owing to the continuity equation, rate of vaporization must equals the  $k_h Q_h$  [ Kim and Srivastava (1988)].

Assuming 10% critical moisture content,

$$k_h Q_h = \frac{h_l A (T_g - T_s)}{H_v}$$

or

$$k_h = \frac{h_l A (T_g - T_s)}{H_v (0.1 Q_s)}$$

Substitute the value of  $k_h$  in moisture balance equation.

$$\frac{1}{v_s} \frac{\partial}{\partial t} Q_h = - \frac{\partial}{\partial z} Q_h - \frac{h_l A (T_g - T_s)}{H_v (0.1 Q_s)}$$

### 3.2.2 Mass balance for the solid

- Rate of flow of solid into the control volume at position  $z$   $= Q_s|_z$
- Rate of flow of solid out of the control volume at position  $z + \Delta z$   $= Q_s|_{z+\Delta z}$
- Rate of consumption of solid due to reaction  $= (\gamma_s)\Delta z$

where  $(\gamma_s)$  rate of reaction per unit length.

$$\gamma_s = -\frac{\partial Q_s}{\partial z} = 6.005 \exp\left(\frac{-8033}{T_s}\right) \frac{Q_a Q_s}{V_s}$$

where,  $Q_a$  is the water vapor flow rate (kg/s)

- Rate of consumption of solid ( in terms of moisture)

due to evaporation of moisture

$$= \frac{h_i A (T_g - T_s) Q_h \Delta z}{H_v (0.1 Q_s)}$$

- Rate of accumulation of the solid

$$= \frac{\Delta}{\Delta t} \left[ Q_s \cdot \frac{\Delta z}{v_s} \right]$$

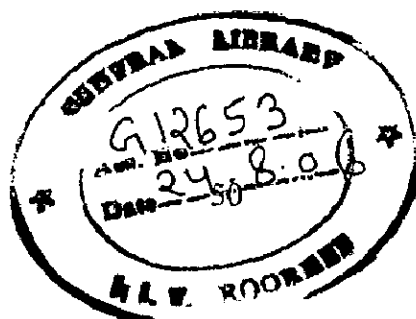
where  $\frac{\Delta z}{v_s} = \Delta \tau$ ; residence time in the control volume.

Applying the balance,

[Rate of flow of solid into the control volume] - [ Rate of flow of solid out from the control volume] - [Rate of consumption of solid within the control volume] = [Rate of accumulation of solid]

$$Q_s|_z - Q_s|_{z+\Delta z} - \left[ 6.005 \exp\left(\frac{-8033}{T_s}\right) \frac{Q_a Q_s \Delta z}{V_s} \right] - \left[ \frac{h_i A (T_g - T_s) Q_h \Delta z}{H_v (0.1 Q_s)} \right] = \frac{\Delta}{\Delta t} \left[ Q_s \cdot \frac{\Delta z}{v_s} \right]$$

divide the above equation by  $\Delta z$



$$-\frac{Q_s|_z - Q_s|_{z+\Delta z}}{\Delta z} - 6.005 \exp\left(\frac{-8033}{T_s}\right) \frac{Q_a Q_s}{V_s} - \frac{h_r A(T_g - T_s) Q_h}{H_v(0.1 Q_s)} = \frac{1}{v_s} \frac{\Delta Q_s}{\Delta t}$$

taking the limit  $\Delta z \rightarrow 0$ ;  $\Delta t \rightarrow 0$

$$-\frac{\partial}{\partial z} Q_s - 6.005 \exp\left(\frac{-8033}{T_s}\right) \frac{Q_a Q_s}{V_s} - \frac{h_r A(T_g - T_s) Q_h}{H_v(0.1 Q_s)} = \frac{1}{v_s} \frac{\partial Q_s}{\partial t}$$

or

$$\frac{1}{v_s} \frac{\partial Q_s}{\partial t} = -\frac{\partial Q_s}{\partial z} - 6.005 \exp\left(\frac{-8033}{T_s}\right) \frac{Q_a Q_s}{V_s} - \frac{h_r A(T_g - T_s) Q_h}{H_v(0.1 Q_s)}$$

### 3.2.3 Mass balance for the gas

- Rate of flow of gas into the control volume at position z =  $Q_g|_z$
- Rate of flow of gas out of the control volume at position z =  $-Q_g|_{z+\Delta z}$
- Rate of consumption of gas =

[rate of consumption of solid] \* [mol. Wt of gas/mol. Wt of solid]

$$= 6.005 \exp\left(\frac{-8033}{T_s}\right) \frac{Q_a Q_s \Delta z}{V_s} \left(\frac{30}{12}\right)$$

- Rate of addition of moisture due to evaporation of moisture within the control volume =  $\frac{h_r A(T_g - T_s) Q_h}{H_v(0.1 Q_s)} \Delta z$
- Rate of accumulation of the gas in the control volume =  $\frac{\Delta}{\Delta t} \left[ Q_g \cdot \frac{\Delta z}{v_s} \right]$

Applying the balances

$$\begin{aligned} & [\text{Rate of flow of gas into the control volume}] - [\text{Rate of flow of gas out from} \\ & \text{the control volume}] - [\text{Rate of consumption of gas within the control volume}] \\ & = [\text{Rate of accumulation of gas}] \end{aligned}$$

$$\begin{aligned} - Q_g|_z - Q_g|_{z+\Delta z} + 6.005 \exp\left(\frac{-8033}{T_s}\right) \frac{Q_a Q_s \Delta z}{V_s} \left(\frac{30}{12}\right) + \frac{h_r A (T_g - T_s) Q_h}{H_v (0.1 Q_s)} \\ = \frac{\Delta z}{v_g} \frac{\Delta}{\Delta t} [Q_g] \end{aligned}$$

divide the above equation by  $\Delta z$  and take the limit  $\Delta z \rightarrow 0$ ;  $\Delta t \rightarrow 0$

$$\begin{aligned} \lim_{\Delta z \rightarrow 0} \frac{Q_g|_{z+\Delta z} - Q_g|_z}{\Delta z} + 6.005 \exp\left(\frac{-8033}{T_s}\right) \frac{Q_a Q_s \Delta z}{V_s} \left(\frac{30}{12}\right) + \frac{h_r A (T_g - T_s) Q_h}{H_v (0.1 Q_s)} \\ = \lim_{\Delta t \rightarrow 0} \frac{1}{v_g} Q_g \end{aligned}$$

Therefore,

$$\frac{\partial}{\partial z} Q_g + 6.005 \exp\left(\frac{-8033}{T_s}\right) \frac{Q_a Q_s \Delta z}{V_s} \left(\frac{30}{12}\right) + \frac{h_r A (T_g - T_s) Q_h}{H_v (0.1 Q_s)} = \frac{1}{v_g} \frac{\partial}{\partial t} Q_g$$

### 3.3 ENERGY BALANCES

Heat is exchanged between solid, gas and wall through conduction, convection and radiation modes. Conduction is important in transmission of heat within the solid as well as from interior of the wall to the outer surface of the shell. For heat transfer in gas to solid and gas to wall, convection mode plays the primary role while radiative heat transfer occurs in all the three phases. Once a phase emits radiation, a fraction of radiation is reflected back to the same phase. Consequently the temperature of the phase depends on its temperature as well as on the other phases. This phenomenon is considered to be the driving force in radiative heat transfer among the phases.

#### 3.3.1 Energy exchange between gas and solid

Energy emitted by the gas	$= \Sigma T_g^4 \epsilon_g$
Energy absorbed by the solid	$= \Sigma T_g^4 \epsilon_g \epsilon_s$
Energy reflected by the solid	$= \Sigma T_g^4 \epsilon_g (1 - \epsilon_s)$
Energy absorbed by the gas	$= \Sigma T_g^4 \epsilon_g (1 - \epsilon_s) \epsilon_g$
Energy reflected by the gas	$= \Sigma T_g^4 \epsilon_g (1 - \epsilon_s)(1 - \epsilon_g)$
Energy absorbed by the solid	$= \Sigma T_g^4 \epsilon_g (1 - \epsilon_s)(1 - \epsilon_g) \epsilon_s$
Energy reflected by the solid	$= \Sigma T_g^4 \epsilon_g (1 - \epsilon_s)^2(1 - \epsilon_g)$
Energy absorbed by the gas	$= \Sigma T_g^4 \epsilon_g^2(1 - \epsilon_s)^2(1 - \epsilon_g)$
And so on.....	

$Q_{net}$  emitted by the gas per unit area,

$$\begin{aligned}
 &= \Sigma T_g^4 \epsilon_g [1 - \{(1 - \epsilon_s)\epsilon_g + \epsilon_g (1 - \epsilon_s)^2(1 - \epsilon_g) + \dots\}] \\
 &= \Sigma T_g^4 \epsilon_g [1 - (1 - \epsilon_s)\epsilon_g \{1 + (1 - \epsilon_s)(1 - \epsilon_g) + \dots\}] \\
 &= \Sigma T_g^4 \epsilon_g [1 - \{(1 - \epsilon_s)\epsilon_g / \{1 - (1 - \epsilon_s)(1 - \epsilon_g)\}\}] \\
 &= \Sigma T_g^4 \epsilon_g [ \{1 - (1 - \epsilon_s)(1 - \epsilon_g) - (1 - \epsilon_s)\epsilon_g\} / \{1 - (1 - \epsilon_s)(1 - \epsilon_g)\}] \\
 &= \{\Sigma T_g^4 \epsilon_g \epsilon_s\} / \{1 - (1 - \epsilon_s)(1 - \epsilon_g)\}
 \end{aligned}$$



Energy emitted by the solid	$= \Sigma T_s^4 \epsilon_s$
Energy absorbed by the gas	$= \Sigma T_s^4 \epsilon_s \epsilon_g$
Energy reflected by the gas	$= \Sigma T_s^4 \epsilon_s (1 - \epsilon_g)$
Energy absorbed by the solid	$= \sigma T_s^4 \epsilon_s (1 - \epsilon_g) \epsilon_s$
Energy reflected by the solid	$= \Sigma T_s^4 \epsilon_s (1 - \epsilon_g)(1 - \epsilon_s)$
Energy absorbed by the gas	$= \Sigma T_s^4 \epsilon_s (1 - \epsilon_g)(1 - \epsilon_s) \epsilon_g$

And so on.....

Energy absorbed by the gas due to solid's radiation

$$\begin{aligned}
 &= \Sigma T_s^4 \epsilon_s \epsilon_g + \Sigma T_s^4 \epsilon_s (1 - \epsilon_g)(1 - \epsilon_s) \epsilon_g + \Sigma T_s^4 \epsilon_s \epsilon_g (1 - \epsilon_g)^2 (1 - \epsilon_s)^2 \\
 &= \Sigma T_s^4 \epsilon_s \epsilon_g [1 + (1 - \epsilon_g)(1 - \epsilon_s) + (1 - \epsilon_g)^2 (1 - \epsilon_s)^2 + \dots] \\
 &= \frac{\sigma T_s^4 \epsilon_s \epsilon_g}{1 - (1 - \epsilon_g)(1 - \epsilon_s)}
 \end{aligned}$$

### 3.3.2 Energy exchange between wall and gas

Energy emitted by the gas	$= \Sigma T_g^4 \epsilon_g$
Energy absorbed by the wall	$= \Sigma T_g^4 \epsilon_g \epsilon_w$
Energy reflected by the wall	$= \Sigma T_g^4 \epsilon_g (1 - \epsilon_w)$
Energy absorbed by the gas	$= \Sigma T_g^4 \epsilon_g (1 - \epsilon_w) \epsilon_g$
Energy reflected by the gas	$= \Sigma T_g^4 \epsilon_g (1 - \epsilon_w)(1 - \epsilon_g)$
Energy absorbed by the wall	$= \Sigma T_g^4 \epsilon_g (1 - \epsilon_w)(1 - \epsilon_g) \epsilon_w$
Energy reflected by the wall	$= \Sigma T_g^4 \epsilon_g (1 - \epsilon_w)^2 (1 - \epsilon_g)$
Energy absorbed by the gas	$= \Sigma T_g^4 \epsilon_g^2 (1 - \epsilon_w)^2 (1 - \epsilon_g)$

And so on.....

$Q_{net}$  emitted by the gas per unit area,

$$\begin{aligned}
 &= \Sigma T_g^4 \epsilon_g [1 - (1 - \epsilon_w) \epsilon_g \{1 + (1 - \epsilon_w)(1 - \epsilon_g) + \dots\}] \\
 &= \Sigma T_g^4 \epsilon_g [1 - \{(1 - \epsilon_w) \epsilon_g\} / \{1 - (1 - \epsilon_w)(1 - \epsilon_g)\}] \\
 &= \{\Sigma T_g^4 \epsilon_g \epsilon_w\} / \{1 - (1 - \epsilon_w)(1 - \epsilon_g)\}
 \end{aligned}$$

Energy emitted by the wall	$= \Sigma T_w^4 \epsilon_w$
Energy absorbed by the gas	$= \Sigma T_w^4 \epsilon_w \epsilon_g$
Energy reflected by the gas	$= \Sigma T_w^4 \epsilon_w (1 - \epsilon_g)$
Energy absorbed by the wall	$= \Sigma T_w^4 \epsilon_w (1 - \epsilon_g) \epsilon_w$
Energy reflected by the wall	$= \Sigma T_w^4 \epsilon_w (1 - \epsilon_g) (1 - \epsilon_w)$
Energy absorbed by the gas	$= \Sigma T_w^4 \epsilon_w \epsilon_g (1 - \epsilon_g) (1 - \epsilon_w)$
Energy reflected by the gas	$= \Sigma T_w^4 \epsilon_w (1 - \epsilon_g)^2 (1 - \epsilon_w)$
Energy absorbed by the wall	$= \Sigma T_w^4 \epsilon_w (1 - \epsilon_g)^2 (1 - \epsilon_w) \epsilon_w$
Energy reflected by the wall	$= \Sigma T_w^4 \epsilon_w (1 - \epsilon_g)^2 (1 - \epsilon_w)^2$
Energy absorbed by the gas	$= \Sigma T_w^4 \epsilon_w \epsilon_g (1 - \epsilon_g)^2 (1 - \epsilon_w)^2$
Energy absorbed by the gas due to wall radiation	

$$= \Sigma T_w^4 \epsilon_w \epsilon_g [1 + (1 - \epsilon_g)(1 - \epsilon_w) + (1 - \epsilon_g)^2 (1 - \epsilon_w)^2 + \dots]$$

$$= \{\Sigma T_w^4 \epsilon_w \epsilon_g\} / \{1 - (1 - \epsilon_g)(1 - \epsilon_w)\}$$

### 3.3.3 Energy exchange between wall and solid due to wall radiation

Energy emitted by the wall	$= A_w \Sigma T_w^4 \epsilon_w$
Energy absorbed by the solid	$= (A_w \Sigma T_w^4 \epsilon_w) \tau_g \epsilon_s F_{ws}$
Energy reflected by the solid	$= (A_w \Sigma T_w^4 \epsilon_w) \tau_g F_{ws} (1 - \epsilon_s)$
Energy absorbed by the wall	$= (A_w \Sigma T_w^4 \epsilon_w) \tau_g F_{ws} (1 - \epsilon_s) \tau_g \epsilon_w$
Energy reflected by the wall	$= (A_w \Sigma T_w^4 \epsilon_w) \tau_g^2 F_{ws} (1 - \epsilon_s) (1 - \epsilon_w)$
Energy absorbed by the solid	$= (A_w \Sigma T_w^4 \epsilon_w) \tau_g^2 F_{ws} (1 - \epsilon_s) (1 - \epsilon_w) \tau_g \epsilon_s F_{ws}$
Energy reflected by the solid	$= (A_w \Sigma T_w^4 \epsilon_w) \tau_g^3 F_{ws}^2 (1 - \epsilon_s)^2 (1 - \epsilon_w)$
Energy absorbed by the wall	$= (A_w \Sigma T_w^4 \epsilon_w) \tau_g^3 F_{ws}^2 (1 - \epsilon_s)^2 (1 - \epsilon_w) \tau_g \epsilon_w$

Net absorbed energy by the wall =  $(A_w \Sigma T_w^4 \epsilon_w) \tau_g (1 - \epsilon_s) F_{ws}$

### 3.3.4 Energy exchange between wall and wall due to wall radiation

$$\begin{aligned}
 \text{Energy emitted by the wall} &= A_w \Sigma T_w^4 \epsilon_w \\
 \text{Energy absorbed by the wall} &= (A_w \Sigma T_w^4 \epsilon_w) \tau_g \epsilon_w F_{ww} \\
 \text{Energy reflected by the wall} &= (A_w \Sigma T_w^4 \epsilon_w) \tau_g (1 - \epsilon_w) F_{ww} \\
 \text{Energy absorbed by the wall} &= [(A_w \Sigma T_w^4 \epsilon_w) \tau_g (1 - \epsilon_w)] F_{ww} \tau_g \epsilon_w F_{ww} \\
 \text{Energy reflected by the wall} &= (A_w \Sigma T_w^4) (1 - \epsilon_w)^2 \tau_g^2 F_{ww}^2 \\
 \text{Energy absorbed by the wall} &= [(A_w \Sigma T_w^4) (1 - \epsilon_w)^2 \tau_g^2 F_{ww}^2] \tau_g \epsilon_w F_{ww}
 \end{aligned}$$

### 3.3.5 Energy exchange between wall and solid due to solid radiation

$$\begin{aligned}
 \text{Energy emitted by the solid} &= A_s \Sigma T_s^4 \epsilon_s \\
 \text{Energy absorbed by the wall} &= A_s \Sigma T_s^4 \epsilon_s \tau_g \epsilon_w \\
 \text{Energy reflected by the wall} &= A_s \Sigma T_s^4 \epsilon_s \tau_g (1 - \epsilon_w) \\
 \text{Energy absorbed by the solid} &= [A_s \Sigma T_s^4 \epsilon_s \tau_g (1 - \epsilon_w)] F_{ws} \tau_g \epsilon_s \\
 \text{Energy reflected by the solid} &= [A_s \Sigma T_s^4 \epsilon_s \tau_g^2 (1 - \epsilon_w)] F_{ws} (1 - \epsilon_s) \\
 \text{Energy absorbed by the wall} &= [A_s \Sigma T_s^4 \epsilon_s \tau_g^2 (1 - \epsilon_w) F_{ws} (1 - \epsilon_s)] \tau_g \epsilon_w \\
 \text{Energy reflected by the wall} &= [A_s \Sigma T_s^4 \epsilon_s \tau_g^3 F_{ws} (1 - \epsilon_w)^2 (1 - \epsilon_s)] \\
 \text{Energy absorbed by the solid} &= [A_s \Sigma T_s^4 \epsilon_s \tau_g^3 F_{ws} (1 - \epsilon_w)^2 (1 - \epsilon_s)] F_{ws} \tau_g \epsilon_s \\
 \text{Energy reflected by the solid} &= [A_s \Sigma T_s^4 \epsilon_s \tau_g^4 F_{ws}^2 (1 - \epsilon_w)^2 (1 - \epsilon_s)^2] \\
 \text{Energy absorbed by the wall} &= [A_s \Sigma T_s^4 \epsilon_s \tau_g^4 F_{ws}^2 (1 - \epsilon_w)^2 (1 - \epsilon_s)^2] \tau_g \epsilon_w
 \end{aligned}$$

Net exchange of heat from the wall by the solid,

$$\begin{aligned}
 &A_w \Sigma T_w^4 \epsilon_w - \left[ \frac{A_w \sigma T_w^4 \epsilon_w^2 \tau_g^2 F_{ws} (1 - \epsilon_s)}{1 - F_{ws} \tau_g^2 (1 - \epsilon_s) (1 - \epsilon_w)} - \frac{A_w \sigma T_w^4 \epsilon_w^2 \tau_g F_{ww}}{1 - F_{ww} \tau_g (1 - \epsilon_w)} \right] - \frac{A_s \sigma T_s^4 \epsilon_s \tau_g \epsilon_w}{1 - \tau_g^2 (1 - \epsilon_s) (1 - \epsilon_s) F_{ws}} \\
 &= A_w \sigma \epsilon_w \left[ 1 - \frac{\tau_g^2 F_{ws} (1 - \epsilon_s)}{1 - F_{ws} \tau_g^2 (1 - \epsilon_s) (1 - \epsilon_w)} - \frac{\epsilon_w \tau_g F_{ww}}{1 - F_{ww} \tau_g (1 - \epsilon_w)} \right] T_w^4 - \frac{A_s \sigma \epsilon_s \tau_g \epsilon_w}{1 - \tau_g^2 (1 - \epsilon_s) (1 - \epsilon_s) F_{ws}} T_s^2
 \end{aligned}$$

$$= A_w[\Phi T_w^4 - \Psi T_s^4]$$

$$\Phi = \sigma \epsilon_w \left[ 1 - \frac{\tau_g^2 F_{ws} (1 - \epsilon_s)}{1 - F_{ws} \tau_g^2 (1 - \epsilon_s)(1 - \epsilon_w)} - \frac{\epsilon_w \tau_g F_{ws}}{1 - F_{ws} \tau_g (1 - \epsilon_w)} \right]$$

$$\Psi = \frac{\left( \frac{A_s}{A_w} \right) \sigma \epsilon_s \tau_g \epsilon_w}{1 - \tau_g^2 (1 - \epsilon_s)(1 - \epsilon_w) F_{ws}}$$

### 3.3.6 Energy balance for the gas

- Rate of the flow of the heat at z due to the flow of gas  $= -Q_g C_p T_g|_z$
- Rate of flow of heat out of the shell at z + Δz due to gas flow  $= -Q_g C_p T_g|_{z+\Delta z}$
- Rate of flow of heat due to convection with in the control volume from gas to solid  $= h_{gs} \Delta z (T_g - T_s) L_{cu}$
- Rate of flow of heat due to convection within the control volume from the gas to wall  $= h_{gw} \Delta z (T_g - T_w) L_{li}$
- Rate of flow of heat due to radiation out, within the control volume from gas to solid  $= \{ \Sigma T_g^4 \epsilon_g \epsilon_s \Delta z L_{cu} \} / \{ 1 - (1 - \epsilon_g)(1 - \epsilon_s) \}$
- Rate of flow of heat due to radiation within control volume from solid to gas  $= \{ \Sigma T_s^4 \epsilon_g \epsilon_s \Delta z L_{cu} \} / \{ 1 - (1 - \epsilon_g)(1 - \epsilon_s) \}$

- Rate of flow of heat due to radiation within control volume from gas to wall  $= \{\Sigma T_g^4 \epsilon_g \epsilon_w \Delta z L_{li}\} / \{1 - (1 - \epsilon_g)(1 - \epsilon_w)\}$
- Rate of flow of heat due to radiation within control volume from wall to gas  $= \{\Sigma T_w^4 \epsilon_g \epsilon_w \Delta z L_{li}\} / \{1 - (1 - \epsilon_g)(1 - \epsilon_w)\}$
- Rate of flow of heat associated with the moisture at position  $z$ , into the control volume  $= C_v(T_s - 373) Q_{h,z}$
- Rate of flow of heat associated with the moisture at position  $z + \Delta z$ , out of the control volume  $= C_v(T_s - 373) Q_{h,z+\Delta z}$
- Rate of accumulation of heat within the control volume  $= \frac{\Delta}{\Delta t} \left[ Q_g C_p T_g \frac{\Delta z}{v_g} \right]$

#### Applying the balances

[Rate of flow of energy into the control volume] - [Rate of flow of energy out from the control volume] - [Rate of consumption of energy within the control volume] = [Rate of accumulation of energy]

$$\frac{\Delta}{\Delta t} \left[ Q_g C_p T_g \frac{\Delta z}{v_g} \right] = - Q_g C_p T_g \Big|_z + Q_g C_p T_g \Big|_{z+\Delta z} - h_{gs} \Delta z (T_g - T_s) L_{cu} - h_{gw} \Delta z (T_g - T_w) L_{li} - \frac{\epsilon_s \sigma L_{cu} \Delta z (T_g^4 \epsilon_g - T_s^4 \epsilon_g)}{1 - (1 - \epsilon_s)(1 - \epsilon_g)}$$

$$- \frac{\sigma L_{vi} \Delta z \epsilon_w (T_g^4 \epsilon_g - T_w^4 \epsilon_g)}{1 - (1 - \epsilon_g)(1 - \epsilon_w)} + C_v(T_s - 373)(Q_{h|z, z} - Q_{h|z})$$

dividing the equation by  $\Delta z$  and take limit  $\Delta z \rightarrow 0$ ,  $\Delta t \rightarrow 0$

$$\frac{1}{V_g} \frac{\partial}{\partial t} (Q_s C_s T_s) = - \frac{\partial}{\partial z} (Q_s C_s T_s) - h_{gs} L_{cu} (T_g - T_s) - h_{ws} L_{vi} (T_g - T_w)$$

$$- \frac{\epsilon_g \sigma L_{cu} \Delta z (T_g^4 \epsilon_g - T_s^4 \epsilon_g)}{1 - (1 - \epsilon_g)(1 - \epsilon_g)} - \frac{\sigma L_{vi} \Delta z \epsilon_w (T_g^4 \epsilon_g - T_w^4 \epsilon_g)}{1 - (1 - \epsilon_g)(1 - \epsilon_w)} + \frac{\partial Q_h}{\partial z} C_v (T - 313)$$

### 3.3.7 Energy balance for the solid

- Rate of flow of heat into the control volume at  $z$  due to the flow of the solid  $= Q_s C_s T_s|_z$
- Rate of flow of heat out of the control volume at  $z + \Delta z$  due to the flow of solid  $= Q_s C_s T_s|_{z+\Delta z}$
- Rate of flow of heat to the solid due to the convection from gas  $= h_{gs} L_{cu} \Delta z (T_g - T_s)$
- Rate of flow of heat to the solid due to the radiation from wall to solid  $= \Phi T_w^4 - \Psi T_s^4$
- Rate of flow of heat to the solid due to the convection from wall to solid  $= h_{ws} L_{cs} \Delta z (T_w - T_s)$

- Rate of flow of heat within the control volume due to gas radiation

$$= \frac{\sigma L_{cu} \Delta z \epsilon_s}{1 - (1 - \epsilon_s)(1 - \epsilon_g)} [T_g^4 \epsilon_g - T_s^4 \epsilon_s]$$

- Rate of flow of heat within the control volume from wall to solid due to convection

$$= h_{ws} L_{cs} \Delta z (T_w - T_s)$$

- Rate of flow of heat within the control volume from wall to solid due to radiation

$$= \Phi T_w^4 - \Psi T_s^4$$

- Rate of consumption of heat due to endothermic reaction within the

control volume

$$= K_e e^{\frac{-8033}{T_s}} \frac{Q_s Q_a}{V_s} \Delta H \Delta z$$

- Rate of accumulation of heat within the control volume

$$= \frac{\Delta}{\Delta t} \left[ Q_s C_s T_s \frac{\Delta z}{V_s} \right]$$

Applying the energy balance,

[Rate of flow of energy into the control volume] - [Rate of flow of energy out from the control volume] - [Rate of consumption of energy within the control volume] = [Rate of accumulation of energy]

$$Q_s C_s T_s \Big|_z - Q_s C_s T_s \Big|_{z+\Delta z} + h_{gs} L_{cu} \Delta z (T_g - T_s) + L_{cu} \Delta z (\Phi T_w^4 - \Psi T_s^4) + h_{ws} L_{cs} \Delta z (T_w - T_s) + \frac{\sigma L_{cu} \Delta z \epsilon_s}{1 - (1 - \epsilon_s)(1 - \epsilon_g)} [T_g^4 \epsilon_g - T_s^4 \epsilon_s] - \left( \frac{\partial Q_H}{\partial z} \right) \Delta z$$

$$- K_e e^{\frac{-8033}{T_s}} \frac{Q_s Q_a}{V_s} \Delta H \Delta z = \frac{\Delta}{\Delta t} \left[ Q_s C_s T_s \frac{\Delta z}{V_s} \right]$$

divide the above equation by  $\Delta z$  and take limit  $\Delta z \rightarrow 0$  and  $\Delta t \rightarrow 0$

$$- \frac{\partial}{\partial z} (Q_s C_s T_s) + C_3 (T_g - T_s) + L_{cu} (\Phi T_w^4 - \Psi T_s^4) + C_7 (T_w - T_s) \\ + C_4 (T_g^4 \epsilon_g - T_s^4 \epsilon_g) - \frac{\partial Q_h}{\partial z} H_v - K_e e^{\frac{-8033}{T_s}} \frac{Q_s Q_a}{V_s} \Delta H = \frac{\partial}{\partial t} (Q_s C_s T_s)$$

where,  $C_3 = h_{gs} L_{cu}$

$$C_4 = \frac{\sigma L_{cu} \epsilon_s}{1 - (1 - \epsilon_s)(1 - \epsilon_g)}$$

$$C_7 = h_{ws} L_{cs}$$

$$C_5 = h_{gw} L_{ic}$$

### 3.3.8 Energy balance for the wall

- Rate of flow of heat into the wall at position  $z$  due to convection from gas

$$= h_g L_{ic} \Delta z (T_g - T_s)$$

- Rate of flow of heat due to radiation within the control

volume from the gas

$$= \frac{\sigma L_{ic} \Delta z \epsilon_w}{1 - (1 - \epsilon_w)(1 - \epsilon_g)} [T_g^4 \epsilon_g - T_s^4 \epsilon_g]$$

- Rate of flow of heat out of the wall due to convection to solid

$$= h_w \Delta z L_{cs} (T_w - T_s)$$



- Rate of flow of heat out of the wall due to radiation to solid =  $L_{cu}\Delta z(\Phi T_w^4 - \Psi T_s^4)$
- Rate of accumulation of heat within the control volume =  $\frac{\Delta}{\Delta t}[M_w C_w T_w \Delta z]$

Applying the balances

[ rate of flow of energy into the control volume] - [ rate of flow of energy out from the control volume] - [ rate of consumption of energy within the control volume ] = [rate of accumulation of energy]

$$\frac{\Delta}{\Delta t}[M_w C_w T_w \Delta z] = h_g \bar{L}_{ic} \Delta z (\bar{T}_g - \bar{T}_s) + \frac{\sigma L_{ic} \Delta z \epsilon_w}{1 - (1 - \epsilon_w)(1 - \epsilon_g)} [\bar{T}_g^4 \epsilon_g - \bar{T}_s^4 \epsilon_g] - h_w \Delta z L_{cs}(T_w - T_s) - L_{cu} \Delta z (\Phi T_w^4 - \Psi T_s^4)$$

divide the above equation by  $\Delta z$  and take limit  $\Delta z \rightarrow 0$

$$- \frac{\partial}{\partial t}(M_w C_w T_w) = h_g L_{ic}(T_g - T_s) + \frac{\sigma L_{ic} \Delta z \epsilon_w}{1 - (1 - \epsilon_w)(1 - \epsilon_g)} [T_g^4 \epsilon_g - T_s^4 \epsilon_g] - h_w \Delta z L_{cs}(T_w - T_s) - L_{cu}(\Phi T_w^4 - \Psi T_s^4)$$

### 3.3.9 Boundary Conditions and Initial Conditions

Initial conditions,

At  $t = 0$ ,

$$\begin{aligned} Q_s(z,0) = Q_s(z), \quad Q_g(z,0) = Q_g(z), \quad Q_h(z,0) = Q_h(z), \\ T_s(z,0) = T_s(z), \quad T_g(z,0) = T_g(z), \quad T_w(z,0) = T_w(z), \quad \text{where } z = [0,L] \end{aligned}$$

Boundary conditions

At  $z = 0$  for  $t \geq 0$

$$Q_h = Q_{ho}, \quad Q_s = Q_{so}, \quad T_s = T_{so}, \quad T_w = T_{wo},$$

At  $z = L$  for  $t \geq 0$

$$Q_g = Q_{gl}, \quad T_g = T_{gl}$$

### 3.4 STEADY STATE MODELS FOR ROTARY REACTOR

The developed model equations are function of two independent variables, viz time (t) and space (z). To make steady state model, characterizing variables depends on time has been neglected. The system of equation become simple coupled ODEs. These equations are

$$\begin{aligned} \frac{\partial Q_h}{\partial z} &= - \frac{h_r A (T_g - T_s) Q_h}{H_v (0.1 Q_s)} \\ \frac{\partial Q_s}{\partial z} &= - K_e e^{\frac{-8033}{T_s}} \frac{Q_a Q_s}{V_s} - \frac{h_r A (T_g - T_s) Q_h}{H_v (0.1 Q_s)} \\ \frac{\partial Q_g}{\partial z} &= K_e e^{\frac{-8033}{T_s}} \frac{Q_s Q_a}{V_s} \frac{30}{12} + \frac{h_r A (T_g - T_s) Q_h}{H_v (0.1 Q_s)} \\ - \frac{\partial}{\partial z} (Q_r C_r T_g) &= C_3 (T_g - T_s) + C_4 (T_g^4 \epsilon_g - T_s^4 \epsilon_g) - C_5 (T_g - T_w) - C_6 (T_g^4 \epsilon_g - T_w^4 \epsilon_g) \\ &\quad + \frac{\partial Q_h}{\partial z} C_v (T_s - 373) \\ \frac{\partial}{\partial z} (Q_s C_s T_s) &= C_3 (T_g - T_s) + C_4 (T_g^4 \epsilon_g - T_s^4 \epsilon_g) + C_7 (T_w - T_s) + L_{cu} (\Phi T_w^4 - \Psi T_s^4) \\ &\quad - \frac{\partial Q_h}{\partial z} H_v - K_e e^{\frac{-8033}{T_s}} \frac{Q_s Q_a}{V_s} \Delta H \\ 0 &= C_5 (T_g - T_w) + C_6 (T_g^4 \epsilon_g - T_w^4 \epsilon_g) - C_7 (T_w - T_s) - L_{cu} (\Phi T_w^4 - \Psi T_s^4) \\ &\quad - Q_{loss} \end{aligned}$$

Boundary conditions

At  $z = 0$  for  $t \geq 0$

$$Q_h = Q_{h0}, \quad Q_s = Q_{s0}, \quad T_s = T_{s0}, \quad T_w = T_{w0}$$

At  $z = L$  for  $t \geq 0$

$$Q_g = Q_{g1}, \quad T_g = T_{g1}$$

### 3.5 Estimation of Reactor's Geometric Parameter

Reactor parameters like chord length of the solid which is exposed to the gas or wall, area of the wall covered by the solid and wall area exposed to the gas or solid are required to calculate the heat transfer. The cross-sectional area for the gas flow and solid flow are needed in calculation of heat transfer coefficient as these coefficients are function of mass velocity of solid and gas. Consider the Figure (3.2) which shows the cross-sectional area of the reactor, solid cross-sectional area are represented by the mesh while empty area represents gas flow area. Solid chord is making an angle of  $\theta$  at the centre of the circle.

$$\text{Area of sector AOBA} = \left(\frac{\theta}{2\pi}\right) * \frac{\pi D^2}{4} = \frac{\theta D^2}{8}$$

Where  $\theta$  is in radian,

$$\text{Area of } \Delta\text{AOM} = \frac{1}{2} \left(\frac{D}{2} \sin\left(\frac{\theta}{2}\right)\right) \left(\frac{D}{2} \cos\frac{\theta}{2}\right)$$

$$= \frac{1}{16} D^2 \left(2 \sin\frac{\theta}{2} \cos\frac{\theta}{2}\right)$$

$$= \frac{1}{16} D^2 \sin\theta$$

$$\text{Area of } \Delta\text{AOB} = \frac{1}{8} D^2 \sin\theta$$

$$\text{Mesh area} = \frac{\theta D^2}{8} - \frac{1}{8} D^2 \sin\theta$$

$$= \frac{D^2}{8} [\theta - \sin\theta]$$

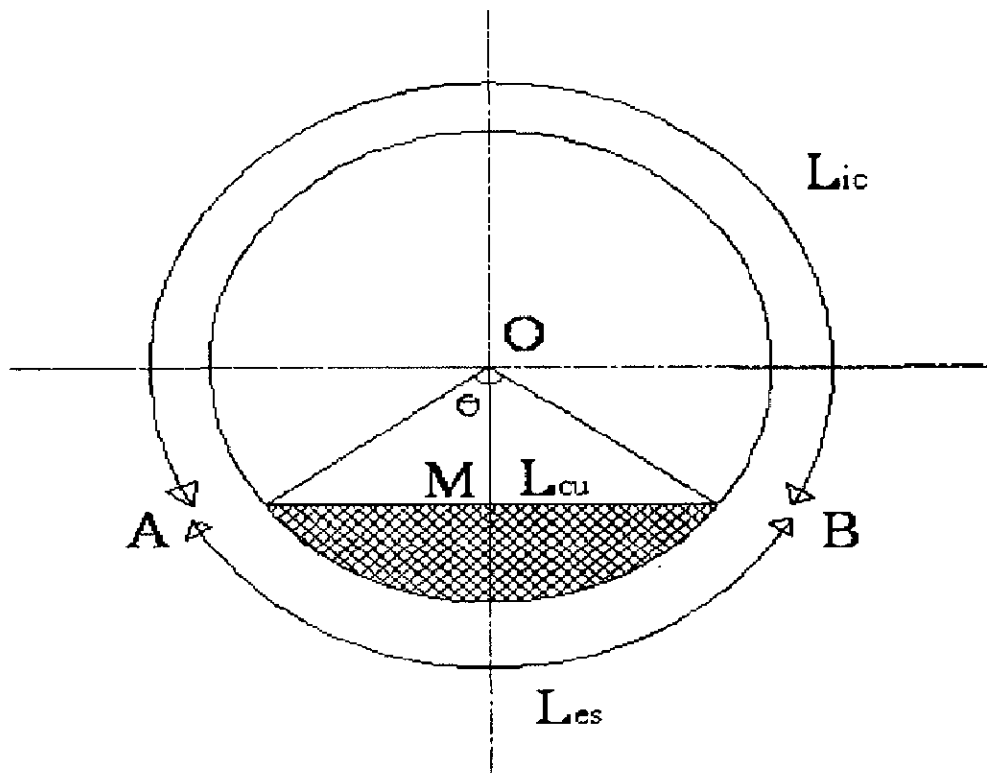


Figure 3.2 Cross-sectional area of the control volume of the reactor

Area in terms of solid flow rate,

$$\text{Area} = \frac{Q_s t}{\rho L}$$

$$\text{But } t = \frac{0.19L}{ND_i S} \quad [\text{Perry (1950)}]$$

$$\begin{aligned} \Rightarrow \text{flow area of solid} &= \frac{Q_s t}{\rho L} \frac{0.19L}{ND_i S} \\ &= \frac{0.19Q_s}{\rho ND_i S} \end{aligned}$$

$$\Rightarrow \frac{0.19Q_s}{\rho ND_i S} = \frac{D^2}{8} [2\theta - \sin \theta]$$

$$\Rightarrow \theta = \frac{1.52Q_s}{\rho ND_i^3 S} + \sin \theta$$

$\theta$  can be calculated numerically. Once  $\theta$  is obtained we can calculate length of solid expose to gas  $L_{cu}$

$$\begin{aligned} L_{cu} &= ZAM \\ &= 2 \left[ \frac{D}{2} \sin \frac{\theta}{2} \right] = D \sin \frac{\theta}{2} \end{aligned}$$

Length of wall covered by solid  $L_{es}$

$$\begin{aligned} L_{es} &= R \theta \\ &= D \theta / 2 \end{aligned}$$

Length of wall exposed to gas  $L_{fi}$

$$\begin{aligned} L_{fi} &= (2\pi - \theta)D/2 \\ &= (\pi - \theta/2)D \end{aligned}$$

For Newton-Raphson method, first approximation of  $\theta$  is as follows

$$\Theta - \sin \theta = \frac{1.52Q_s}{\rho ND_i^3 S}$$

$\sin \theta$  can be expanded in a series of  $\theta$

$$\Rightarrow \theta - \sin \theta = \theta - \left( \theta - \frac{\theta^3}{3!} + \frac{\theta^5}{5!} - \frac{\theta^7}{7!} + \dots \right) = \frac{1.52 Q_s}{\rho N D_i^3 S}$$

$$= \left( \frac{\theta^3}{3!} + \frac{\theta^5}{5!} - \frac{\theta^7}{7!} + \dots \right) + 0(\text{higher order terms}) = \frac{1.52 Q_s}{\rho N D_i^3 S}$$

$$\approx \left( \frac{\theta^3}{3!} \right) = \frac{1.52 Q_s}{\rho N D_i^3 S}$$

$$\Rightarrow \theta = \frac{1}{D_i} \sqrt[3]{\frac{9.12 * Q_s}{\rho * NS}}$$

### RESULTS AND DISCUSSIONS

---

---

#### 4.1 INTRODUCTION

It is assumed that the solid bed moves as a pseudo fluid with axial displacement and without back mixing and rolls in the transverse direction as the cylinder rotates. The geometric parameters i.e.  $L_{es}$ ,  $L_{cu}$ , and  $L_{fi}$  were determined as a function of solid flow rate, residence time and rotary reactor dimension by means of geometric relationship and iterative method as described in Chapter III.

#### 4.2 Algorithm

The computation of the state of the rotary reactor requires the solution of five non-linear first order Ordinary Differential Equations (ODE) and two non-linear algebraic equations along large set of variable parameter formulas. The solution of algebraic equation is computed by means of Newton-Raphson algorithm. The algorithm is implemented in 300 lines of program and 415 words in Matlab (7.0 Version). The boundary conditions are inputs of the reactor i.e. the flow rate of solid and moisture content of the solid at the solid input end of the reactor and gas flow rate and temperature at the solid output end. The RKF method is used for integration method. The algorithm is proposed by assuming that the temperature and flow rate of the gas at the solid input end and integrate forward for both gas and material. The temperature and flow rate of the gas were modified as long as the boundary conditions for the gas at the solid output end were not matched, and the process repeated until the solid output end boundary condition was satisfied. The algorithm is summarized as follows:

*Step 1:* The value of reactor dimensions and constants that are independent of state variables viz. heat of reaction, heat of vaporization, water vapor flow rate and thermal conductivity of solid and initial conditions are given as input.

*Step 2:* Assume the temperature and flow rate of gas at the solid input end.

*Step 3:* Calculate the dependent variables viz. emissivity, thermal properties of the gas and solid, geometric parameters of the reactor, heat transfer coefficients and view factor.

*Step 4:* Integrate the system of equations in the forward direction using RKF algorithm of appropriate step size.

*Step 5:* Compute the temperature of the wall using computed value of gas and solid temperature and flow rate.

*Step 6:* Repeat step 5 until the end of reactor length.

*Step 7:* Compare the temperature and flow rate of gas at the solid output end with the boundary conditions. Check whether the boundary conditions of the gas are satisfactory. If not, assume a new value of the temperature and flow rate of the gas.

### **4.3 CHARCOAL ACTIVATION**

The wood is the principal raw material of the process. The wood is fed on the upper section of rotary reactor and it flows along the length of reactor due to gravitational force so that in the following figures the start of x-axis is the upper section of the reactor.

#### **4.3.1 Data and correlations**

Density of solid ( $\text{kg/m}^3$ ) = 864

Length of reactor (m) = 3.7

Rotational speed of reactor (rpm) = 2

Slope of reactor ( $\tan \theta$ ) = 0.05;

Internal diameter of the reactor (m) = 0.3

Thermal conductivity of solid ( $\text{w/m}^2\text{-K}$ ) = 0.207677

Heat of vaporization of water ( $\text{J/kg}$ ) = 2257200

Water vapor flow rate ( $\text{kg/sec}$ ) = 0.005

Solid flow rate ( $\text{kg/sec}$ ) = 0.00333

Initial Moisture content of solid ( $\text{kg/sec}$ ) = 10% of solid

Initial temperature of solid (K) = 500

Initial temperature of wall (K) = 620



Heat capacity of water vapor (kcal/kg) (Dumont and Belanger, 1978)

$$= 8.22 + 0.000015T_g + 0.00000134T_g^2$$

Emissivity of solid (Perry) = 0.895

Emissivity of wall (Perry) = 0.93

Emissivity of gas (Dumont Belanger, 1978) =  $0.85 - 0.0005T_g$

Residence time (sec) = 6480

Heat capacity of solid (J/kg) = 2380

Thermal conductivity of gas ( $W/m^2-K$ ) (Derived from Perry)

$$= -3E-8T_g^2 + 9.8E-4T_g - 0.000267$$

Heat capacity of gas (kJ/kg) (Derived from Perry) =  $3E-7T_g^2 - 0.0001T_g + 0.9893$

Viscosity of gas (Derived from Perry) =  $5E-6T_g^3 - 0.0025T_g^2 + 6.0001T_g - 91.121$

Gas to solid heat transfer coefficient ( $W/m^2-K$ ) (Gorog *et al.* 1982) =  $0.4G_g^{0.8}$

Gas to wall heat transfer coefficient ( $W/m^2-K$ ) (Gorog, *et al.* 1982)

$$= 0.036 \left( \frac{k_s}{d_i} \right) Re^{0.8} Pr^{0.33} \left( \frac{d_i}{l} \right)^{0.035}$$

Wall to solid heat transfer coefficient ( $W/m^2-K$ ) (Gorog, *et al.* 1982) =  $\frac{11.6k_s}{d_i s} \left( \frac{nr_i^2 s}{30k_s} \right)^{0.3}$

### 4.3.2 Flow profile along the length of reactor

Figure (4.1) shows the variation of moisture content of the solid along the length of the reactor. It is clear that the moisture content decreases linearly which is obvious because drying of the solid is directly proportional to the moisture content of the solid. The slope of the curve is decreasing linearly until the onset of chemical reaction that occurs at approximately 2.5 m from the solid input end, because the solid contains critical moisture and the heat gain by the solid in this range is utilized in the vaporization

process. At the onset of the reaction, the slope decreased exponentially with respect to length which is expected because reaction is of first order.

Figure (4.2) represents the gas flow rate profile along the length of the reactor. The gas enters at 3.7m counter-currently with solid flow. The reaction commences as the gas comes in contact with solid and leads to the release of carbon dioxide which mixes and moves with incoming gas. This flow rate continues to increase exponentially. At the length of 2.5m of the reactor, the temperature of the solid is less than 1073 K and no reaction occurs. This makes the gas flow rate constant

Figure (4.3) shows the solid flow rate profile along the length of the reactor. The solid flow rate is nearly constant up to a length of 2.5 m and only moisture vaporization is observed in this range. Due to first order reaction kinetics of solid with respect to length of the reactor, the solid flow rate decreased exponentially and continued up to the exit of the reactor. The reaction started at a temperature of 1073 K and solid achieved this temperature at a distance of 2.5 m. The solid in the reactor never reached above 1273 K which is other extreme limit of reaction and so the solid continued to decrease.

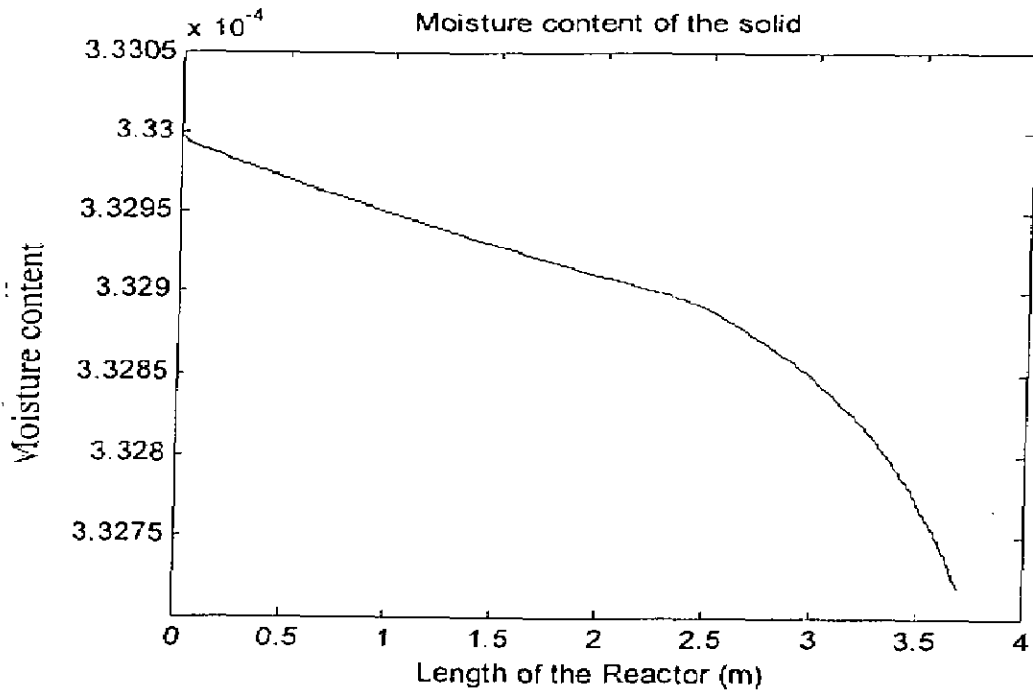


Figure 4.1 Moisture profile along the length

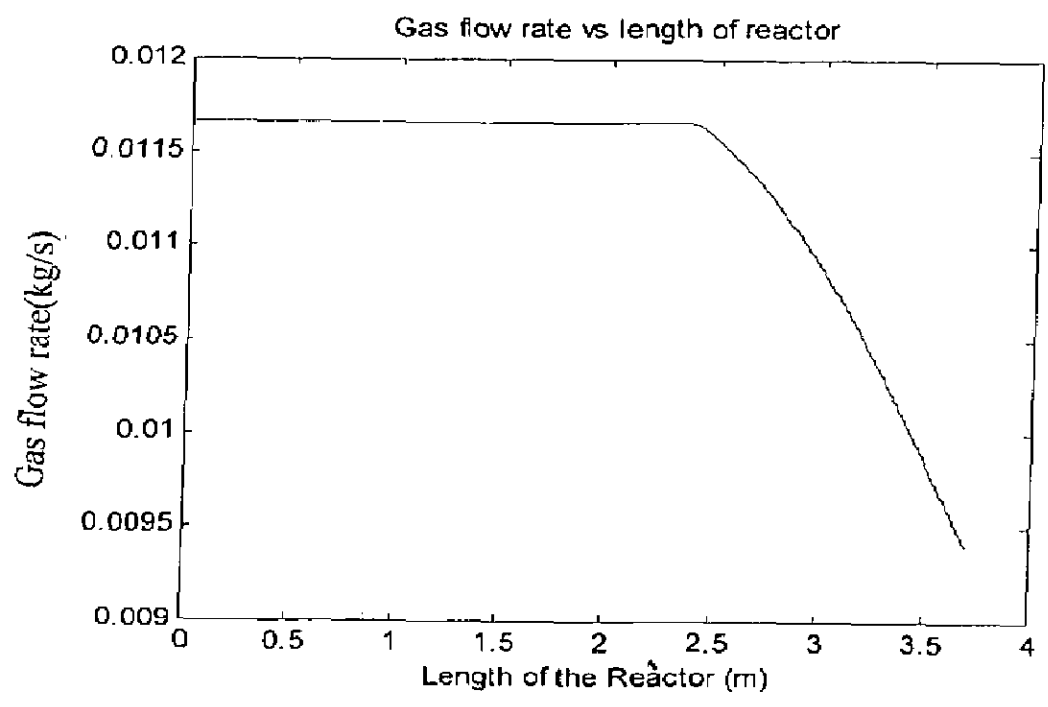


Figure 4.2 Gas flow profile along the length

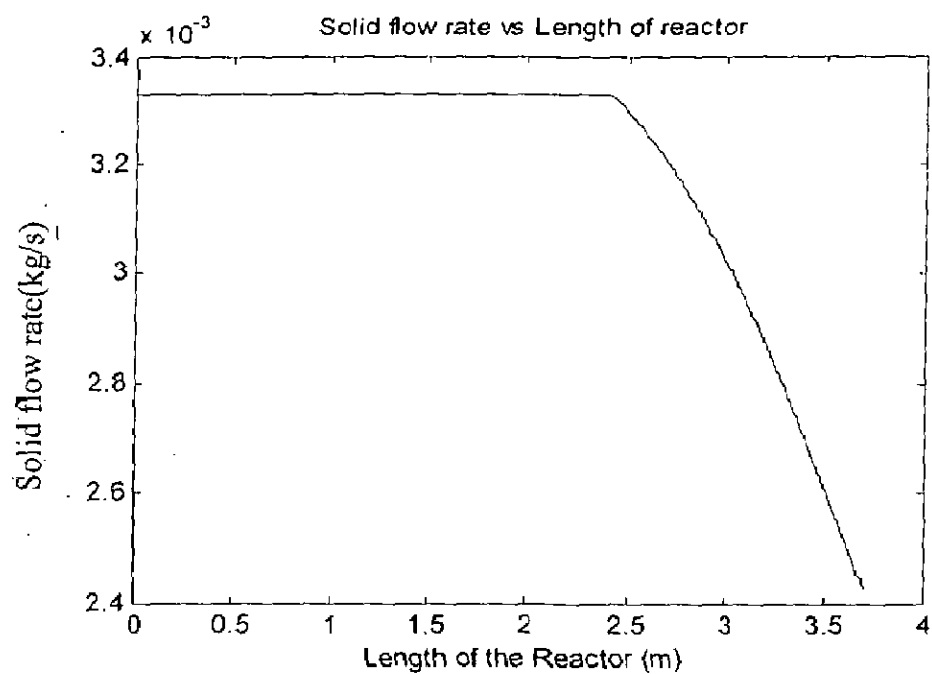


Figure 4.3 Solid flow profile along the length

### 4.3.3 Temperature profile along the length of reactor

Axial gas temperature profile is shown in Figure (4.4). The gas average temperature decreases with the decreasing slope from the solid output end (which is the input end for gas) of the reactor with the operating range of 750-1381 K. Activation reaction started at 2.5 m from solid input end, beyond this range the gas temperature profile gives higher slope, because of highly endothermic reaction. On the other hand during the final stage of the reactor, the gas heat flux is utilized to raise the temperature of solid to the reaction temperature and to remove the moisture.

Axial temperature profile for the solid is mentioned in Figure (4.5). The temperature of the solid approached to the gas temperature and sudden rise of temperature in the initial stage is because of higher temperature driving force. At this end solid enters at 500 K and the gas exits at 750 K. The experimental value of solid temperature signifies that gas to solid heat transfer is low, while the simulated value which is higher signifies that the used correlation predict higher value of heat transfer coefficient. Figure (4.7) shows that the solid temperature crossed the wall temperature within 0.1m length of the reactor and continues at higher value up to the onset of reaction. At a length of 2.5 m of the reactor the solid temperature become constant for a short length of reactor that is the onset of reaction. During this short length the heat flux received by solid is balanced by the endothermic heat of reaction.

Axial temperature profile of wall is shown in Figure (4.6). The temperature of the wall is almost identical to the solid temperature through out the reactor. In the reaction zone wall temperature is slightly higher than the solid temperature. It was assumed that overall heat transfer coefficient from wall to air is constant. The overall heat transfer coefficient varies with temperature, it may be less at lower temperature and high at higher temperature. Therefore the simulated wall temperature profile shows low value as compared to experimental value in the initial stage while higher in the later stage.

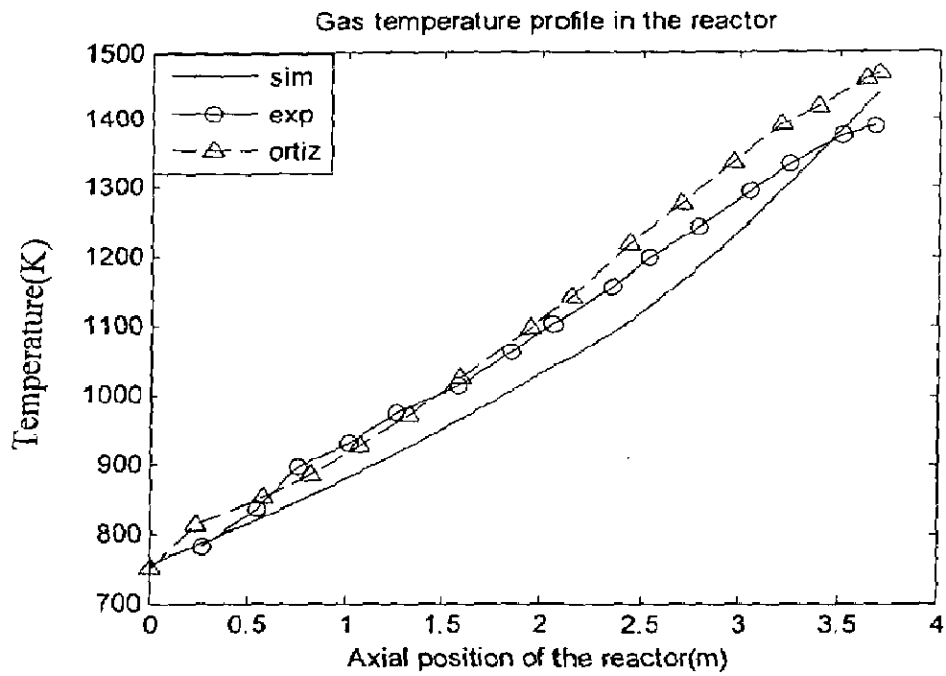


**Figure 4.4 Gas temperature profile along the length of reactor**

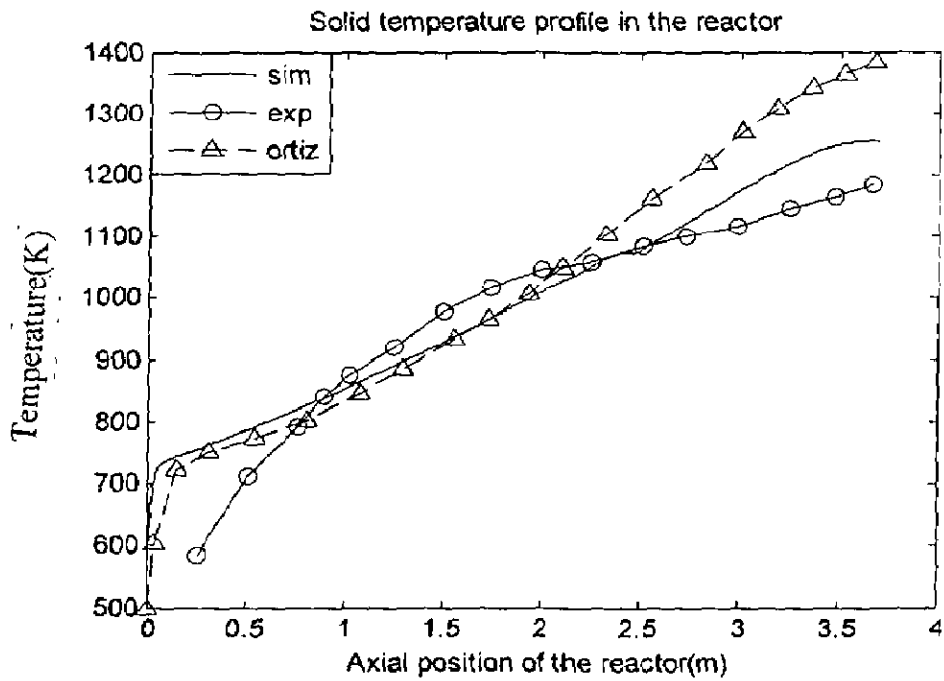


**Figure 4-5 Solid temperature profile along the length of reactor**

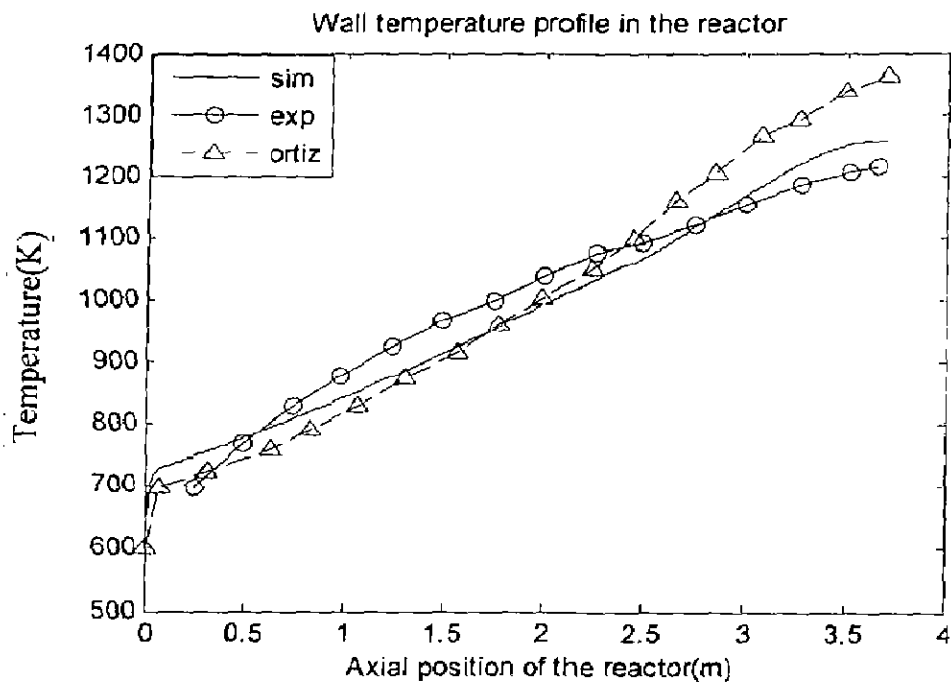


Figure 4.6 Wall temperature profile along the length of reactor

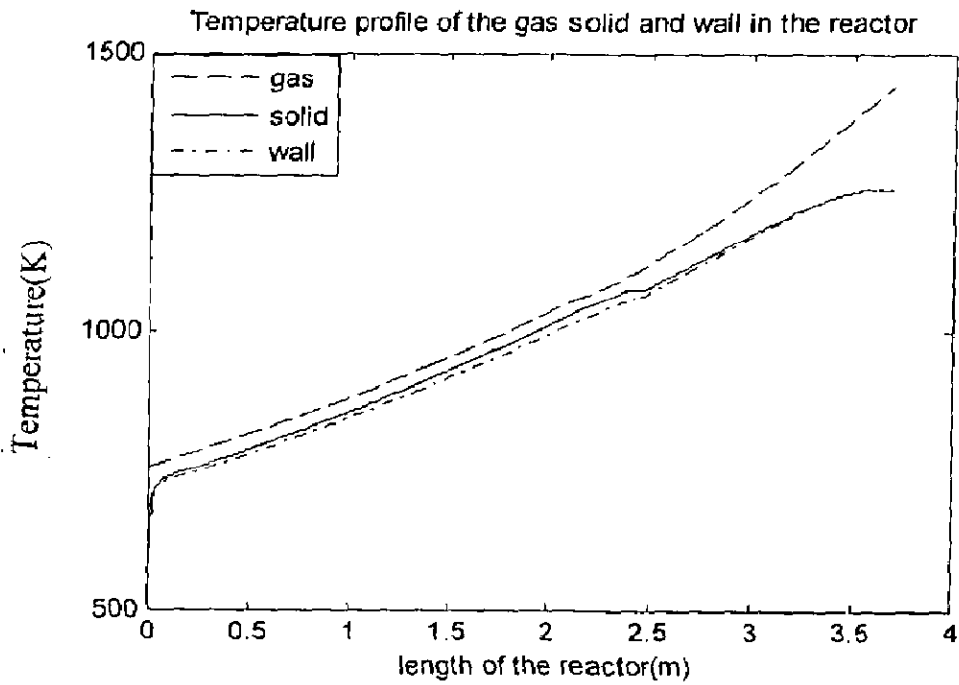


Figure 4.7 Temperature profile of solid wall and gas in the reactor

## 4.4 CALCINATIONS OF LIMESTONE

Calcium oxide (lime) is one of the most used raw materials for different process industries: construction, steel manufacture, chemical processes, environmental protection etc. In soda ash manufacture, both limestone decomposition process products are needed: gaseous flow (carbon dioxide for carbonation of ammoniacal brine) and solid flow (lime for ammonia recovery from waste water coming from the carbonation columns).

Mathematical modeling and simulation at steady state conditions of the horizontal rotary reactor represents a valuable tool for studying different construction design approaches, operating strategies, control system design configurations, improvement of the product quality and for decreasing the energy consumptions.

The thermal decomposition of limestone is a very important process. In 2002, 116000 thousand metric tonnes of lime was produced in the entire world [Cormos]. Lime, the main product of limestone thermal decomposition process, is a basic chemical. Practically the lime is used in every human activity domain. The breakdown of consumption by major end users is as follows: 36 % for metallurgical use, 27 % for environmental use, 24 % for chemical and industrial use and 13 % for construction use (data presented are for year 2002).

### 4.4.1 Data and correlations

Density of solid ( $\text{kg/m}^3$ ) = 1680

Length of reactor (m) = 5.5

Rotational speed of reactor (rpm) = 1.5

Slope of reactor ( $\tan \theta$ ) = 0.03;

Internal diameter of the reactor (m) = 0.406

Thermal conductivity of solid ( $\text{w/m}^2\text{-K}$ ) = 0.69

Heat of vaporization of water ( $\text{J/kg}$ ) = 2257200

Solid flow rate ( $\text{kg/hr}$ ) = 42



Initial Moisture content of solid (kg/sec) = 10% of solid

Initial temperature of solid (K) = 550

Initial temperature of wall (K) = 550

Heat capacity of water vapor (kcal/kg) (Dumont, Belanger, 1978)

$$= 8.22+0.000015T_g+0.00000134T_g^2$$

Emissivity of solid (Perry) = 0.95

Emissivity of wall (Perry) = 0.95

Emissivity of gas (Dumont and Belanger, 1978) = 0.85-0.0005T<sub>g</sub>

Residence time (sec) = 5400

Heat capacity of solid (J/kg) = 1040

Thermal conductivity of gas (W/m<sup>2</sup>-K) (Derived from Perry)

$$= -3E-8T_g^2+9.8E-4T_g-0.000267$$

Heat capacity of gas (kJ/kg) (Derived from Perry) = 3E-7T<sub>g</sub><sup>2</sup>-0.0001T<sub>g</sub>+0.9893

Viscosity of gas (Derived from Perry) = 5E-6T<sub>g</sub><sup>3</sup>-0.0025T<sub>g</sub><sup>2</sup>+6.0001T<sub>g</sub>-91.121

Gas to solid heat transfer coefficient (W/m<sup>2</sup>-K) (Gorog *et al.* 1982) =  $0.4G_k^{0.8}$

Gas to wall heat transfer coefficient (W/m<sup>2</sup>-K) (Gorog, *et al.* 1982)

$$= 0.036\left(\frac{k_g}{d_i}\right) Re^{0.8} Pr^{0.33}\left(\frac{d_i}{l}\right)^{0.055}$$

Wall to solid heat transfer coefficient (w/m<sup>2</sup>-K) (Gorog, *et al.* 1982) =  $\frac{11.6k_s}{d_{,s}}\left(\frac{nr_i^2s}{30\kappa_i}\right)^{0.3}$

The simulation of the mathematical model of the limestone thermal decomposition process reveals the evolution of temperature and flows of solid and gaseous products distribution in a horizontal rotary reactor.

Some of the most representative simulation results are presented in the figures below. The limestone is the principal raw material of the process, the feed of limestone is on the upper end of horizontal rotary reactor, so that in the figures below the axis marked

"0" is the solid input end. The horizontal rotary reactor is divided in three major zones. The first zone is the heating zone for the solid phases (a mixture of limestone and moisture) and at the same time the cooling zone for the gaseous phase. The second zone is the thermal decomposition zone of the limestone, carbon dioxide generated in the process is transferred from the solid phase to gas phase. The third zone is again heating zone for the solid phase (lime) and the cooling zone for the gaseous phase (air) that enters into the reactor.

#### **4.4.2 Flow profile along the length of reactor**

Figures (4.8), (4.9) and (4.10) present the gas, moisture and limestone flow profiles along the length of reactor. The flows are constant in the heating and cooling zones (for gas) of the reactor, because in these zones only physical processes occurs (heat transfer between solid, gaseous phase and reactor wall) without mass transfers between the gases and solids presented in the reactor. The decomposition of calcium carbonate leads to decreasing in solids flow in the reaction zone which can be observed from the Figure (4.10) at a distance of 1 m. Also the gas flow increases along the reaction zone because of carbon dioxide formation in the process. The calcination stopped at 3m of the reactor beyond that the solid gas flow rate became constant.

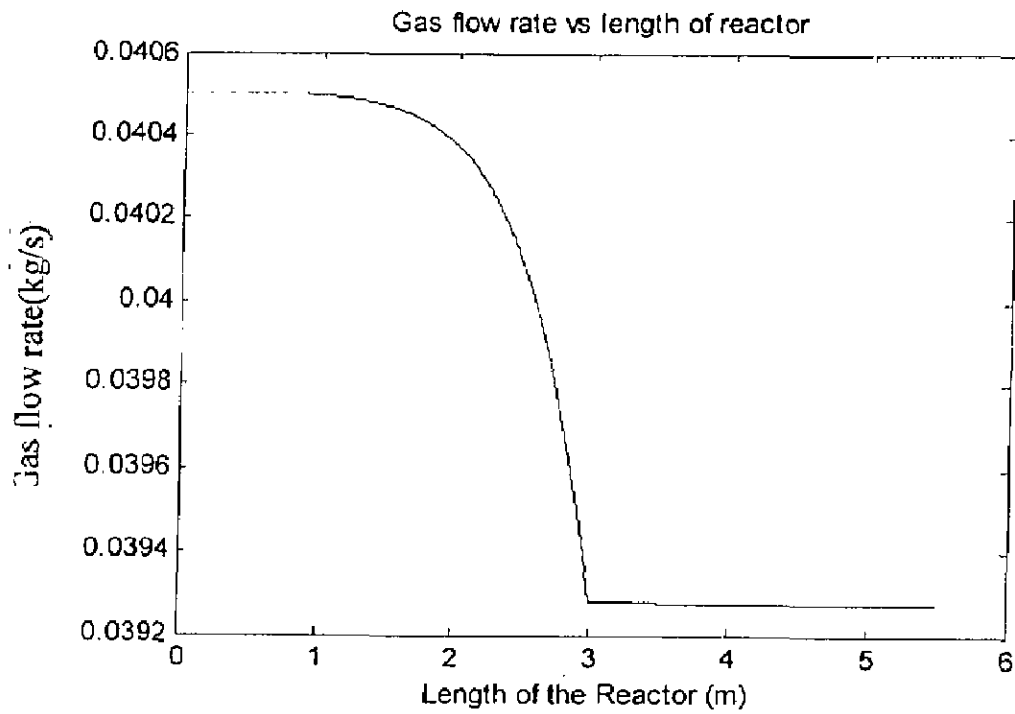


Figure 4.8 Gas flow profile along the length of Reactor

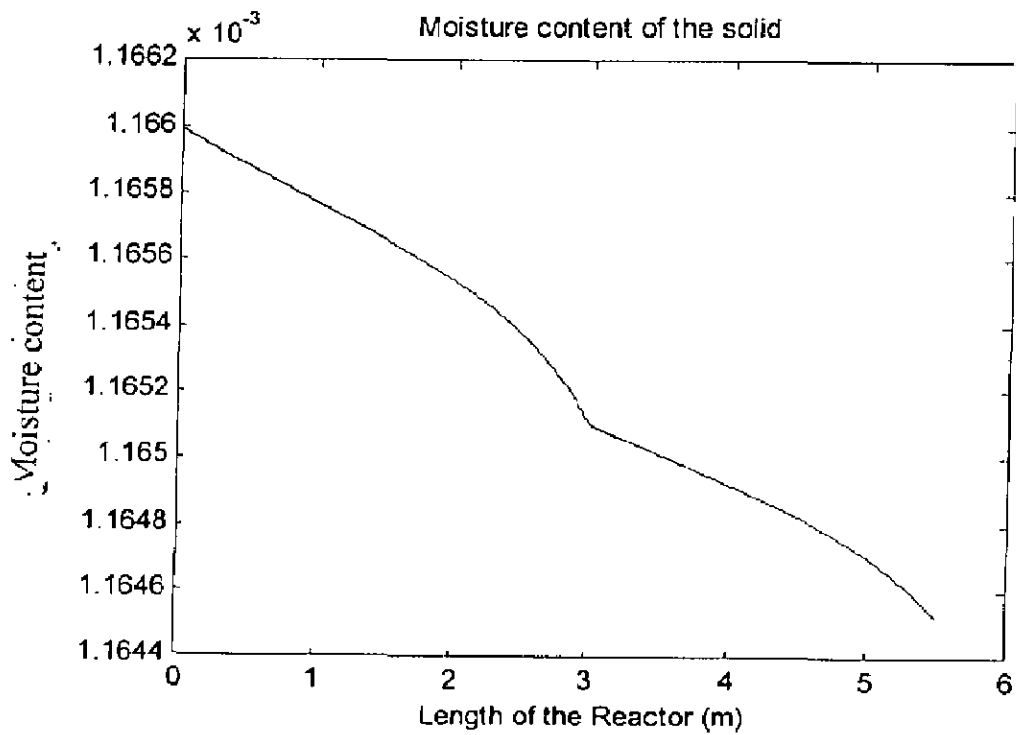


Figure 4.9 Moisture flow profile along the length of Reactor

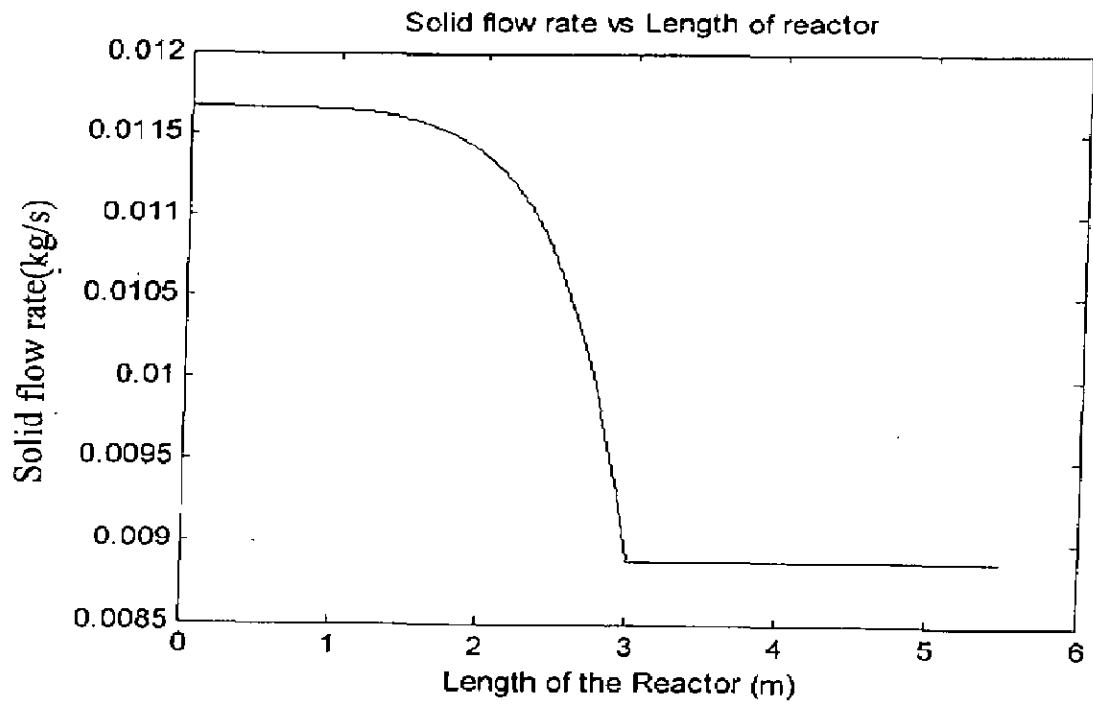


Figure 4.10 Solid flow profile along the length of Reactor

#### 4.4.3 Temperature profile along the length of reactor

By solving the energy balance equations of the process, the profiles of temperatures along the reactor length can be determined. The gas temperature ( $T_g$ ), the limestone ( $\text{CaCO}_3 + \text{CaO}$ ) temperature ( $T_s$ ), and the inside reactor wall temperature ( $T_w$ ) profiles are presented in the Figures (4.11), (4.12), and (4.13).

Figure (4.12) shows that the solid temperatures increases in the heating zone. Limestone is introduced the upper end of the reactor while solids are heated by the hot gaseous phase, leaving the reaction zone up to the point when limestone thermal decomposition begins (around 900 K). The lime resulted in the decomposition zone again encountered with the hot gases, but due to domination of reaction enthalpy the slope of the profile becomes low. The sudden temperature rise in the simulated result at the end of reaction zone is because of forward difference method of integration. In the third zone the gaseous phase (air) is introduced at the lower end of the reactor. The maximum temperature of solid is in the third zone in which lime is heated with counter-current flow of hot gas that is about 1600 K. In the second zone, where the calcination reaction takes place, the maximum temperature is 1200 K which is the upper limit of reaction. The axial temperature profile shows that the peak freeboard gas temperature reached ~1800 K. The simulated results show a little lower temperature than the experimental value. Owing to large temperature difference the gas temperature underwent rapid cooling in the later stage of the reactor. The wall temperature profile follows the gaseous and solid phases profiles along the length of the reactor.

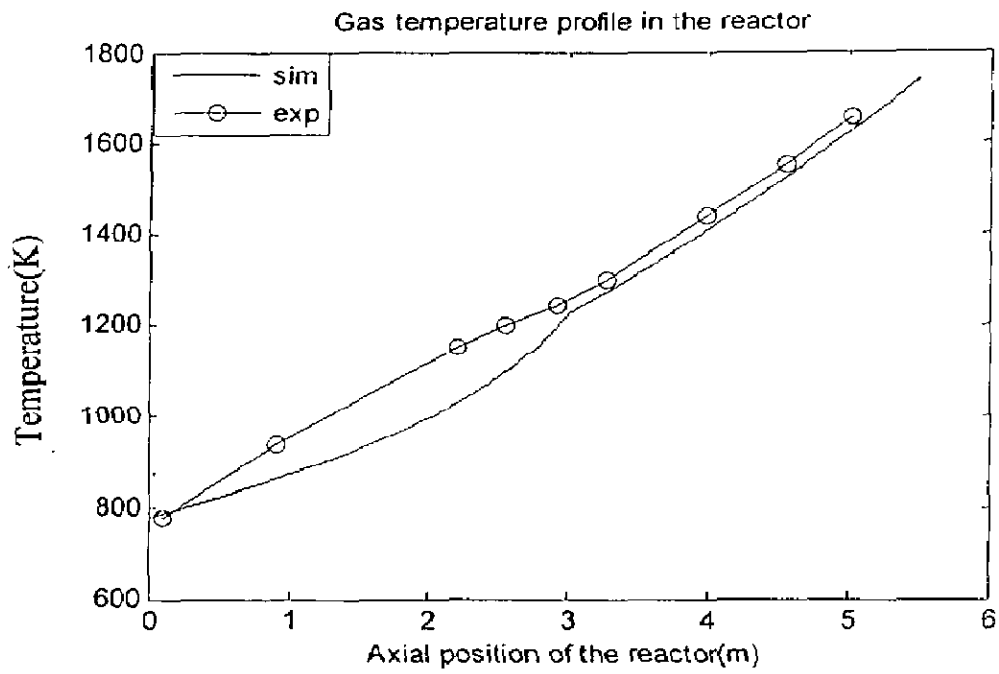


Figure 4.11 Gas temperature profile

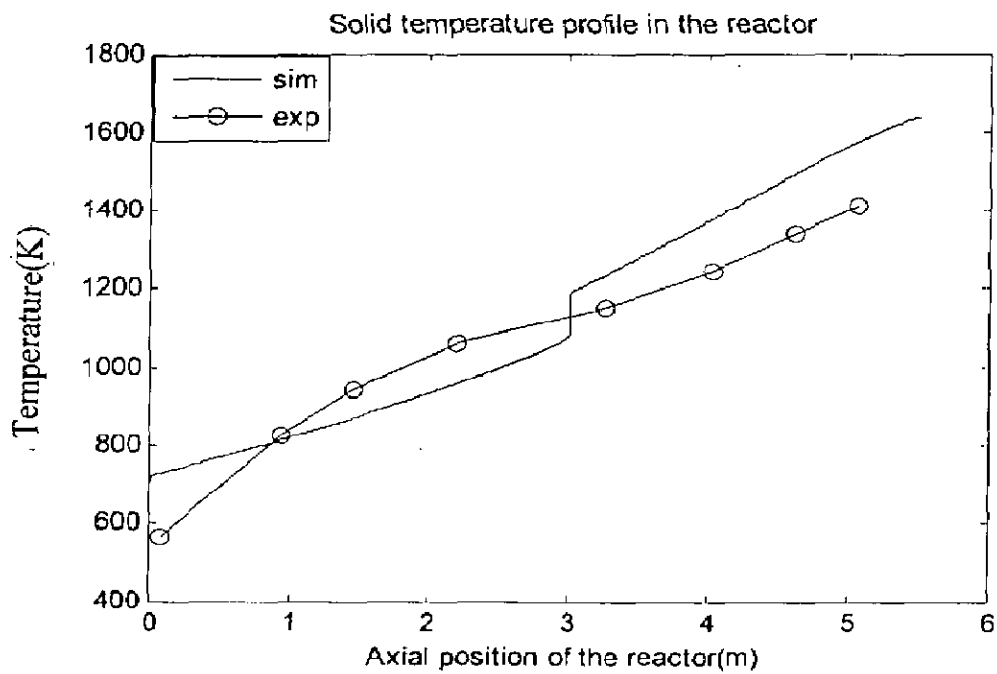


Figure 4.12 Solid Temperature Profile

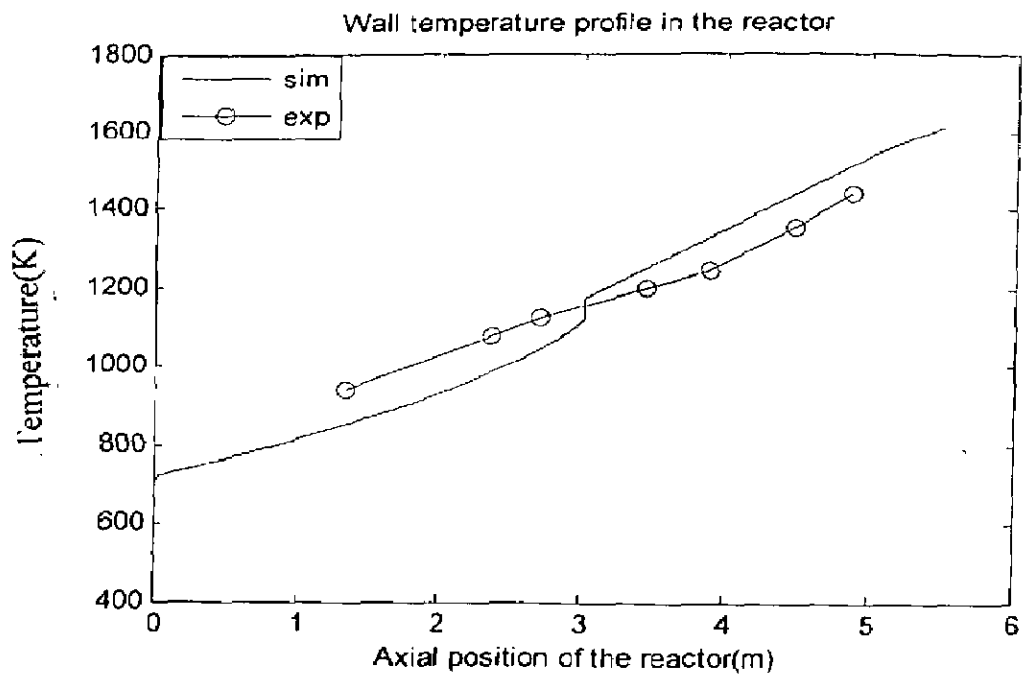


Figure 4.13 Wall Temperature Profile

#### 4.5 SENSITIVITY ANALYSIS

The residence time, vapor flow rate, gas flow rate and solid flow rate plays an important role in the production and burn off. The production and burn off have been defined by Ortiz *et. al.*, 2003a.

$$\text{Burn off [\%]} = 100 \left( \frac{Q_{s,o} - Q_{s,out}}{Q_{s,o}} \right)$$

$$\text{Production [\%]} = 100 \left( \frac{Q_{s,out}}{Q_{s,o}} \right)$$

It can be observed from the Figures (5.1) and (5.4) that the increase in residence time and solid flow rate decrease the production and increases the burn off because the reactants gets more time in the reactor. This implies that more will be the conversion while water vapor is one of the reactant whose increment increases the burn off and reduces production. On the other hand the effect of solid input temperature is insignificant which is obvious from Figure (5.3). On increasing gas flow rate and solid flow rate, production becomes 100 % and burn off 0% because solid under that condition cannot achieve the reaction temperature and no reaction occurs. Figure (5.5) shows that burn off decreases and production increases because of insignificant gas flow rate. Figure (5.2) show that for given conditions of simulation, increment in gas flow rate reduces the burn off to 0% and production to 100%.



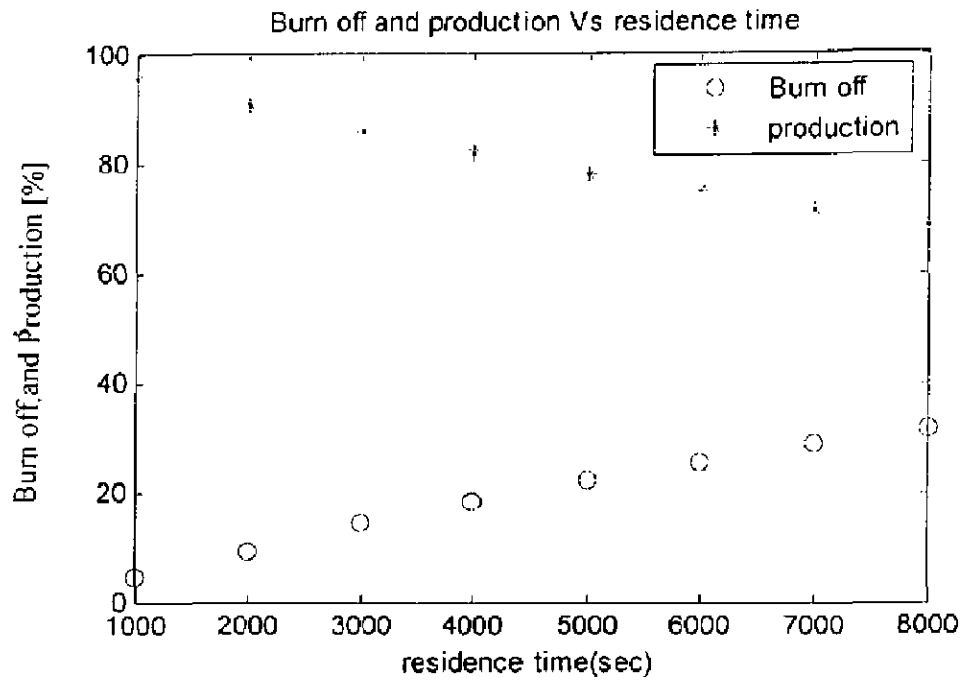


Figure 5.1 Burn off and production Vs residence time

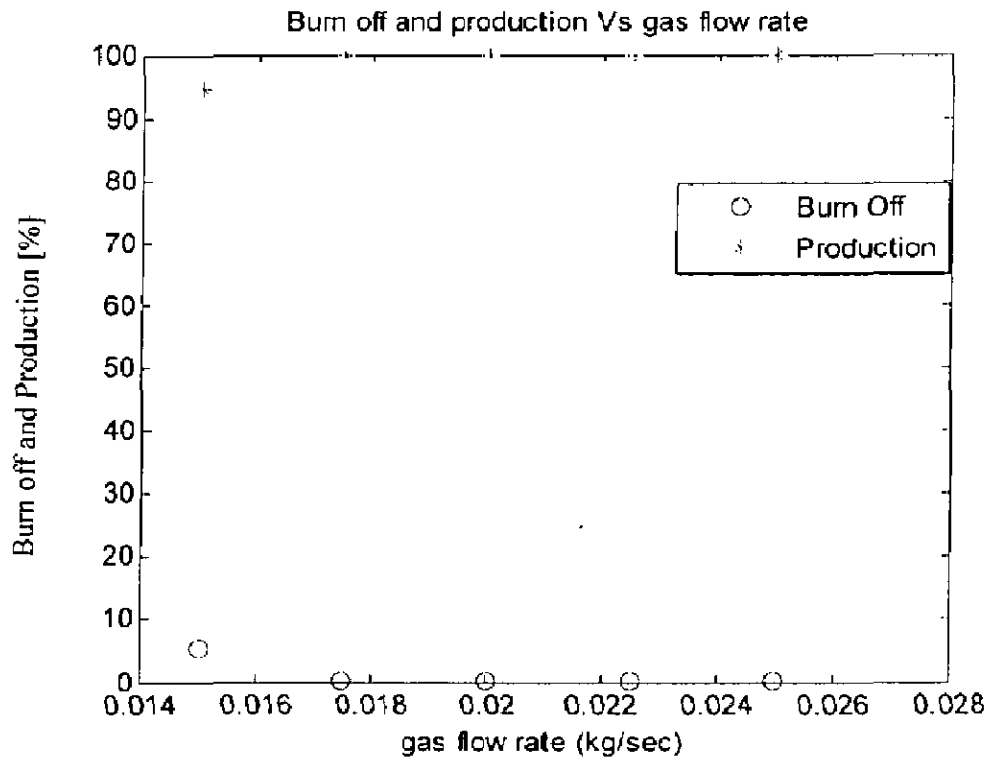


Figure 5.2 Burn off and production Vs gas flow rate

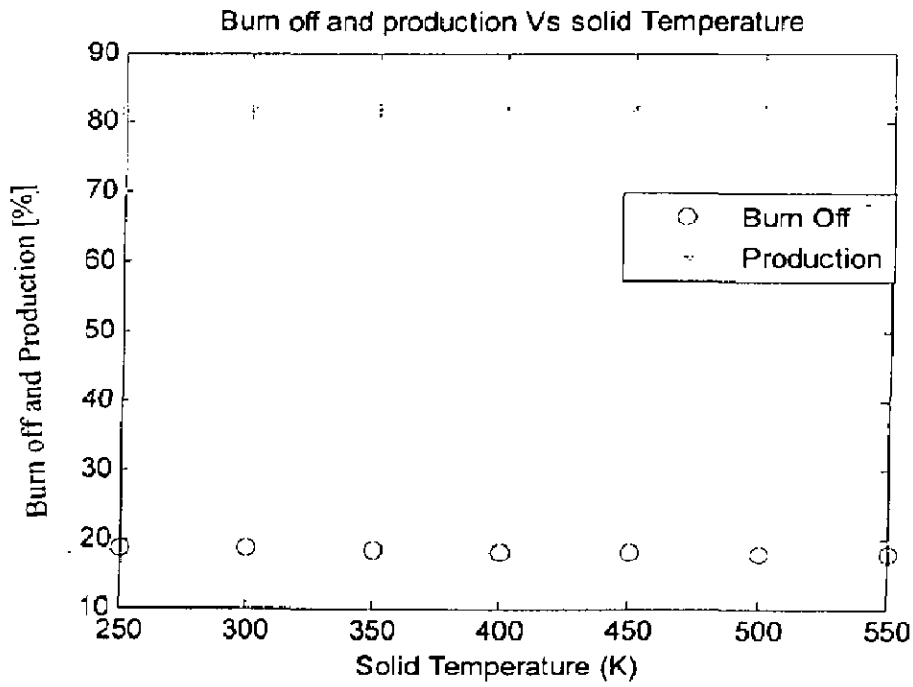


Figure 5.3 Burn off and production Vs solid input temperature

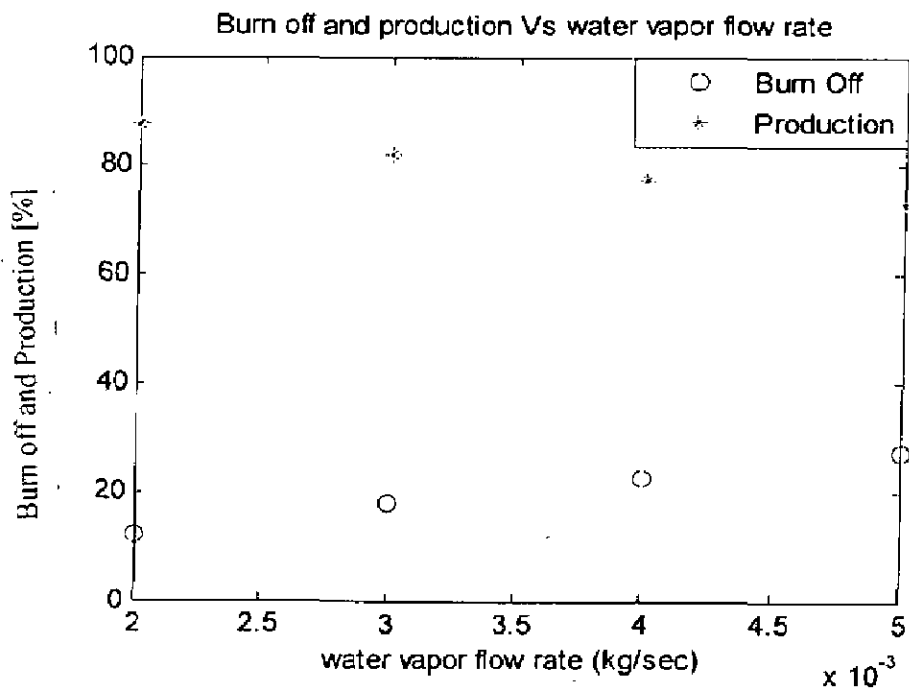


Figure 5.4 Burn off and production Vs water vapor flow rate

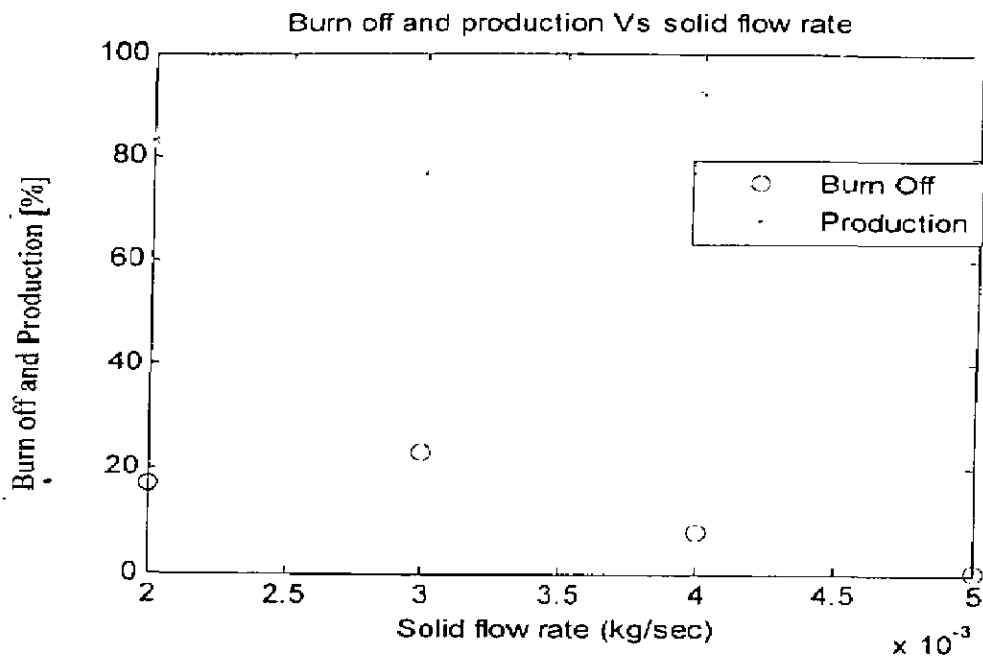


Figure 5.5 Burn off and Production Vs solid flow rate

**CONCLUSIONS AND RECOMMENDATIONS**

---

---

**5.1 CONCLUSIONS**

The physical and chemical processes occurring inside the rotary reactor are very complex. To establish the technical feasibility of the rotary reactor a model has been developed. This model is based on mass and energy balances. The important conclusions derived from the study are as follows:

- The temperatures of the bed material and inside reactor wall were found to be coupled closely.
- A very rapid heating occurred within the initial 0.1m length of the reactor.
- At the onset of reaction the heat input to the bed material and heat consumed by the reaction are same for short length of reactor.
- The extent of calcination is determined by the temperature reached by the bed material. The temperature of solid depends on the rate of heat transfer to the bed.
- An estimation of heat transfer coefficient is quite difficult because of reliable experimental data, while wall to solid heat transfer is dominated by convection.
- Residence time, water vapor flow rate, solid flow rate and gas flow rate are found to be important parameters. Therefore these operating variables can be considered as optimization variables.

## 5.2 RECOMMENDATIONS OF FUTURE WORK

Though the proposed model is in good agreement with the experimental values of two different reactions, more rigorous models are required to understand the operation of a rotary kiln. The guidelines for future work in modeling of rotary kiln are as follows:

- The model should incorporate all the operating variables as a function of characterizing variable.
- The model should incorporate the regenerative effect of the wall.
- Heat transfer in longitudinal direction should be taken into account..
- The model should incorporate various types of motion of particles inside the reactor.
- Because the freeboard gases are common to rotary reactor operations and the gas contains  $\text{CO}_2$  and  $\text{H}_2\text{O}$ , these mixtures should be consider as real gas.
- A more reliable heat transfer coefficient between solid and wall or gas is required.

## REFERENCES

- Barr, P.V. Brimcombe, J.K., Watkinson, A.P. (1989) "A heat transfer model for the Rotary Kiln: Part I. Pilot Kiln Trails.", *Metallurgical Transaction*, 20B, 391-402.
- Boateng, A. A. & Barr, P.V. (1996) "A thermal model for the rotary kiln including heat transfer within the bed", *Int. J. Heat Transfer*, 39, 2131-2147.
- Boateng, A.A. and Barr, P.V. (1996) "A thermal model for the rotary kiln including heat transfer within the bed", 39, 2131-2147.
- Chakrabarti, B.K. (2002) "Investigations on heat loss through the kiln shell in magnesite dead burning process: a case study", *Applied Thermal Engineering*, 22, 1339-1345.
- Cormos, A.M., Ph.D. Thesis, Faculty of Chemistry and Chemical Engineering, "Babes-Bolyai" University of Cluj, Napoca (2005)
- Dumont, G. and Belanger, P.R. (1978) "Steady State Study of Titanium Dioxide Rotary Kiln", *Ind. Eng. Chem. Process Des. Dev.*, 17, No,2, 107-113.
- Gorog, J.P., Adams, T.N. and Brimacombe, J.K. (1982) "Regenerative Heat Transfer in Rotary Kilns", *Matallurgical Transaction*, 13B, 153-163.
- Kim, N.K., Srivastava, R. (1988) "Simulation of an industrial Rotary Calciner with trona ore decomposition", *Ind. Eng. Chem. Res.* 27, 1194-1198.
- Li, S.Q., Chi, Y., Li, R.D., Yan, J.H. and Cen, K.F. (2002) "Axial transport and residence time of MSW in rotary kilns: Part II. Theoretical and optimal analyses", *Powder Technology*, 126, 228-240.

Luisser, M. Ph.D. Thesis , Technical University Viene (2004)

Marias, F. (2003) "A model of a rotary kiln incinerator including processes occurring within the solid and the gaseous phases", *Computer and Chemical Engineering*, 27, 813-825.

Martins,M.A., Oliveira,L. S.,Franca, A.S. (2001) "Modelling and simulation of petroleum coke calcination in rotary kilns", *Fuel*, 80, 1611-1622.

Meier, A. Bonaldi,,E., Cella, G.M., Lipinski, W.,Wuillemin, D. and Palumbo, R. (2004) "Design and experimental investigation of a horizontal rotary reactor for the solar thermal production of lime", *Energy*, 29, pp 811-821.

Mellmann, J. (2001) "The transverse motion of solids in the rotating cylinders- forms of motion and transition behaviour", *Powder Technology*, 118, 251-270.

Munitius, A., Kurcyusz,E., and Kaweck,W. (1974) "Mathematical Model of the Aluminum Oxide Rotary Kiln", *Ind.Eng. Chem. Process Des Develop*, 13(2), 132-142

Ortiz, O.A., Martínez, N.D. and Noriega, S.E. (2003a) "Steady state simulation of rotary kiln for charcoal activation", *Latin American Applied Research*, 33, 51-57.

Ortiz, O.A., Martínez, N.D.,Mengual, S.E.,Petkovic,L.M. (2003b) "Performance analysis of rotary kiln for activated charcoal manufacturing, using a steady state mathematical model.", *Latin American Applied Research*, 33, 2051-210.

Ortiz, O.A., Suarez, G.I. and Nelson, A. (2005) "Dynamic simulation of pilot rotary kiln for charcoal activation", *Computer and Chemical Engineering*, 29, 1837-1848.

Palmer, G. (1998) "Heat transfer in rotary kiln", Proceedings to Cement Industry Federation Technical Conference.

Perry, J.H., (1950) *Chemical Engineers Handbook* (3<sup>rd</sup> ed.) McGraw Hill.

Santomaso, A., Olivi, M. and Canu, P.(2005) "Mixing kinetics of granular material in drums operated in rolling and cataracting regime", *Powder Technology*, 152, 41-51.

Sheritt, G.R., Chaouki, J., Mehrotra, A.K. and Behie, L.A.(2003) "Axial dispersion in the three dimensional mixing of particles in the rotating drum reactor", *Chemical Engineering Science*, 58, 401-415.

Sofialidis, D., Faltsi, O., Sardi, K., Skevis, G., Skodras, G., Kaldis, S.P. and Sakellaropoulos, G. (2005) "Modelling low-temperature carbonisation of solid fuels in a heated rotary kiln for clean fuel production", *Fuel* (Article in press)

Takafumi, S., Kurosawa, S., Smith, R.L., Adschiri, T., Arai, K., (2004) "Water gas shift reaction kinetics under noncatalytic conditions in supercritical water", *The journal of supercritical fluids*, 29, 113-119.

Van Dijen, F.K., Metselaar, R. (1989) "Chemical reaction engineering aspects of a rotary reactor for carbothermal synthesis of SiC" *Journal of European Ceramic Society*, 5, 55-61.

Watkinson, A.P., and Brimacombe, J.K. (1982), "Limestone calcination in rotary kiln", *Metallurgical Transactions*, 13B, 369-378.

Wes, G.W.J., Drinkenburg, A.A.H. and Stemerding, S. (1976) "Heat Transfer in a Horizontal Rotary Drum Reactor", *Powder Technology*, 13, 185-192.